From pore to process: ultra-efficient SF_6/N_2 continuous separation using inexpensive robust MOF composites

Jinjian Li,[a,1] Yuting Chen,[a,1] Tian Ke,[a,*] Liu Yang,[a,b] Zhiguo Zhang,[a,b] Zongbi Bao,[a,b] Qilong Ren,[a,b] Qiwei Yang[a,b,*]

[a]Key Laboratory of Biomass Chemical Engineering of Ministry of Education, College of Chemical and Biological Engineering, Zhejiang University, Hangzhou 310027, Zhejiang, China.

[b]Institute of Zhejiang University-Quzhou, Quzhou 324000, Zhejiang, China.

[*]Corresponding author. Email: yangqw@zju.edu.cn, ketian@zju.edu.cn.

[1]These authors contributed equally to this work.

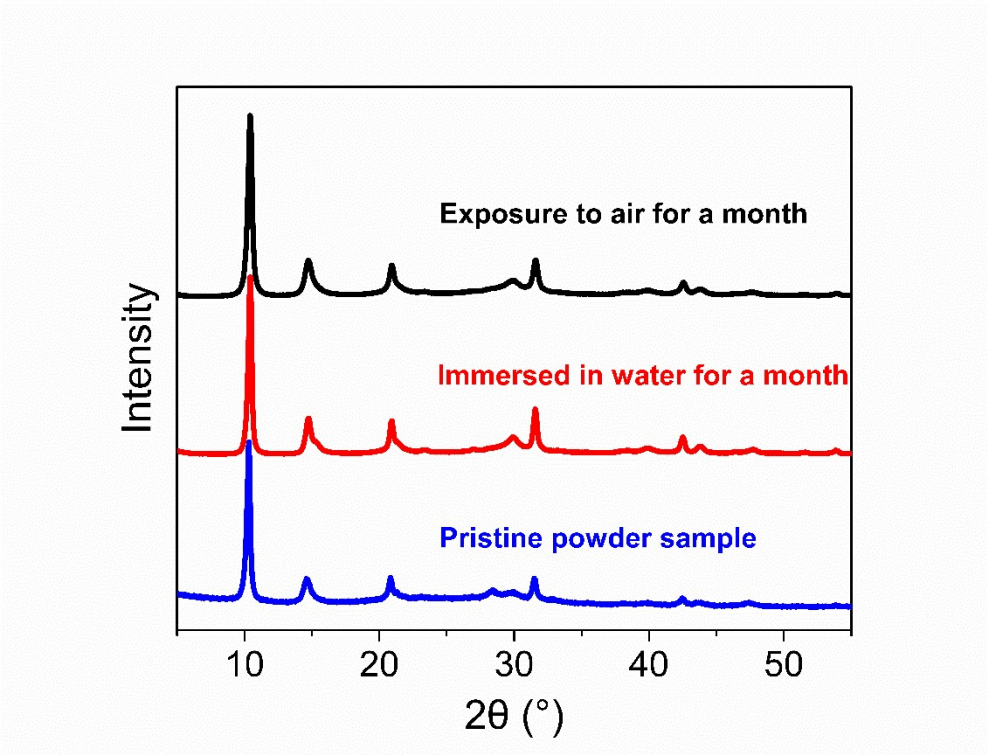

Supplementary Fig. 1 Powder X-ray diffraction patterns of Al(fum).

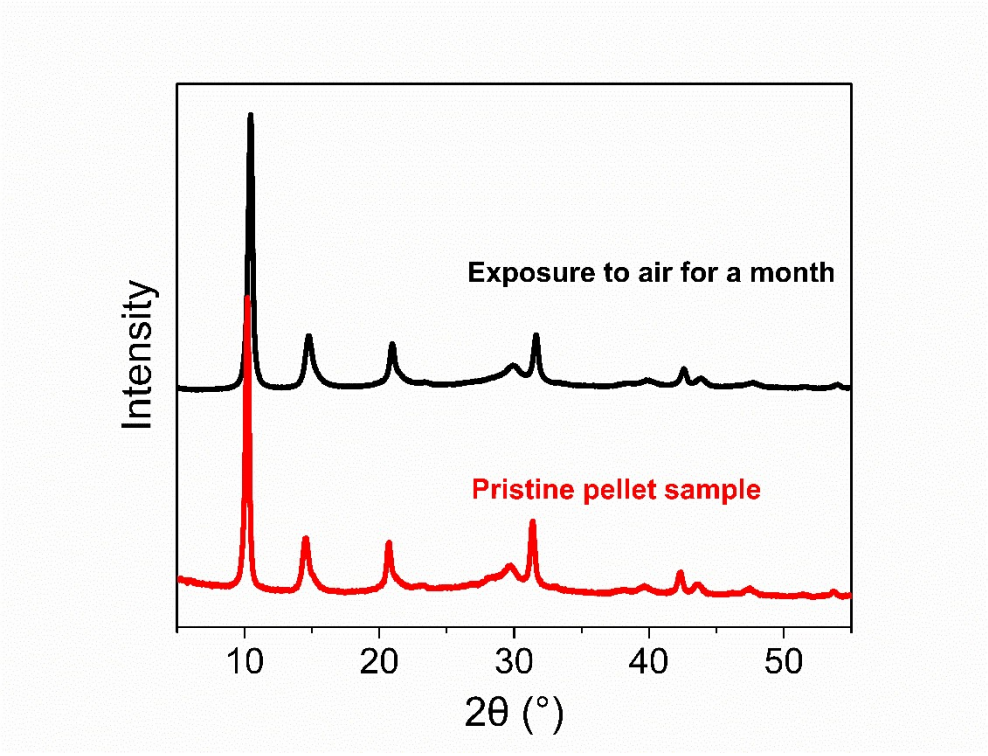

Supplementary Fig. 2 Powder X-ray diffraction patterns of Al(fum)@2%HPC.

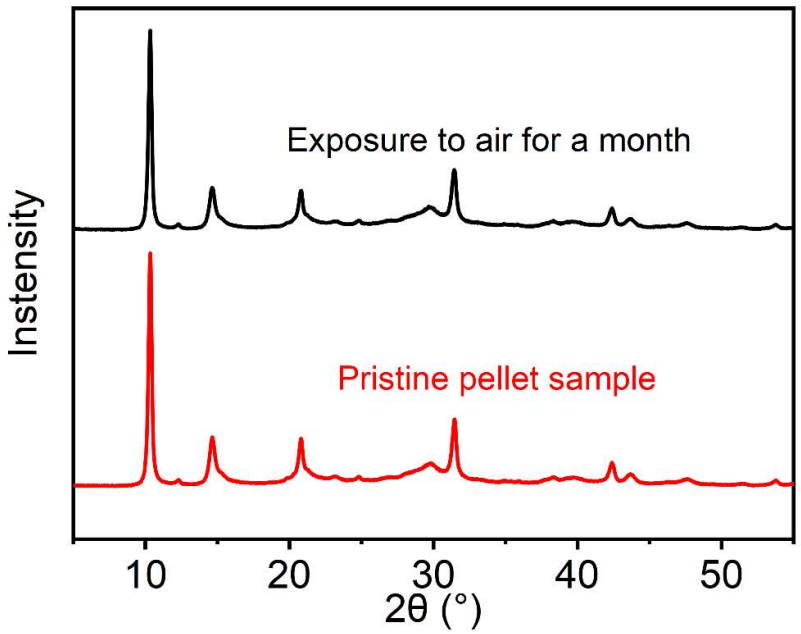

Supplementary Fig. 3 Powder X-ray diffraction patterns of Al(fum)@5%Kaolin.

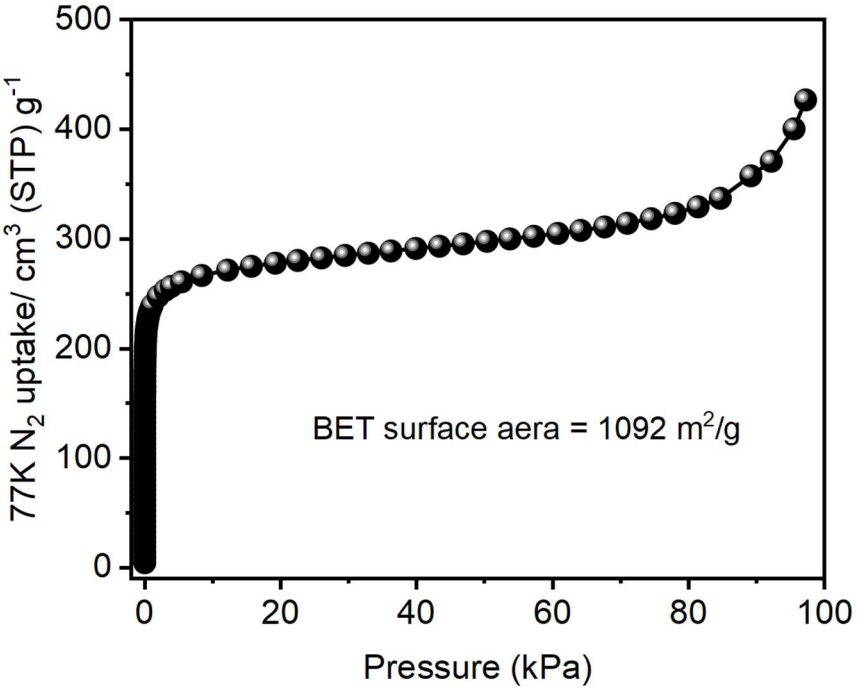

Supplementary Fig. 4 N_2 adsorption isotherm at 77 K of Al(fum).

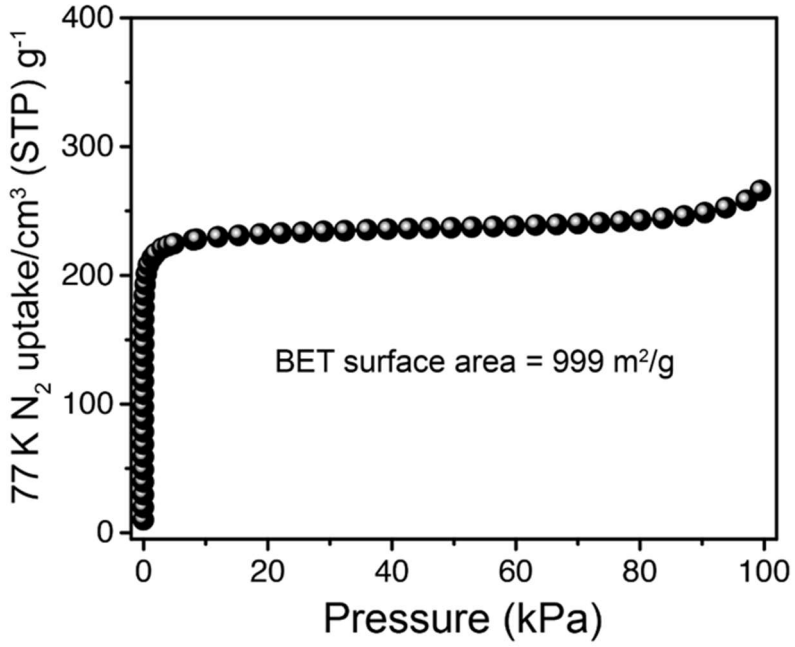

20

21 **Supplementary Fig. 5** N_2 adsorption isotherm at 77 K of Al(fum)@2%HPC.

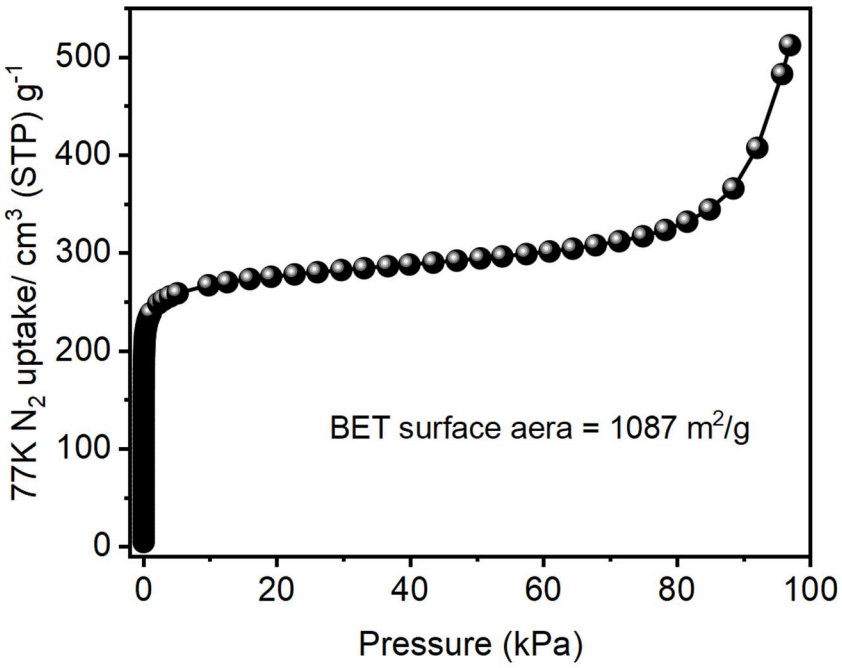

22

23 **Supplementary Fig. 6** N_2 adsorption isotherm at 77 K of Al(fum)@5%Kaolin.

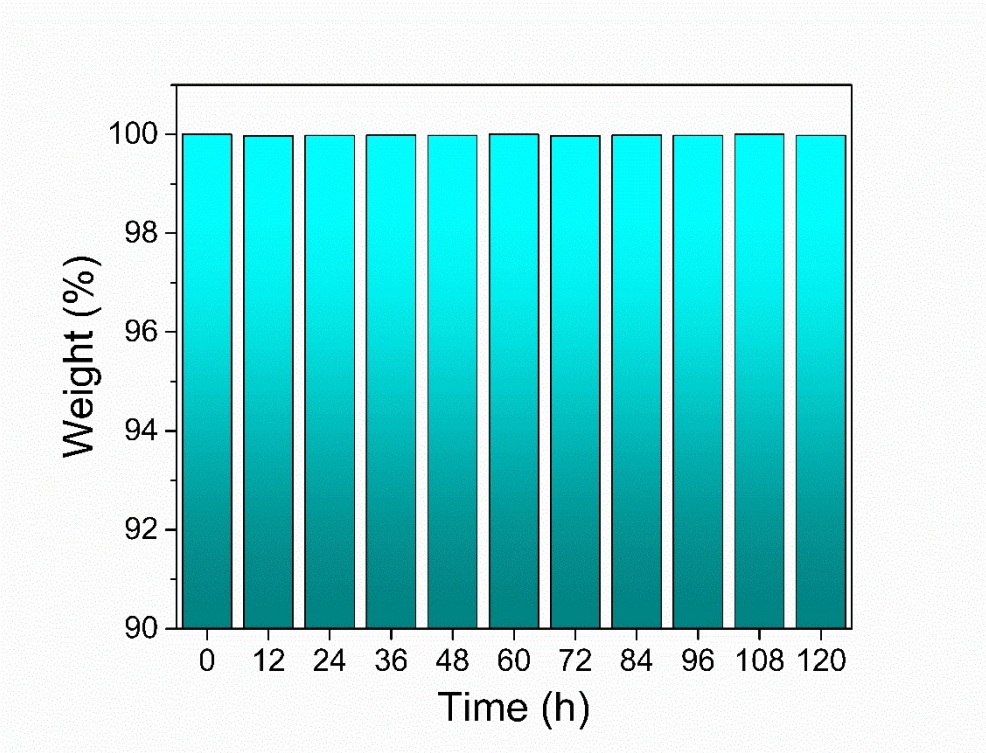

Supplementary Fig. 7 Simulated abrasion test of Al(fum)@2%HPC.

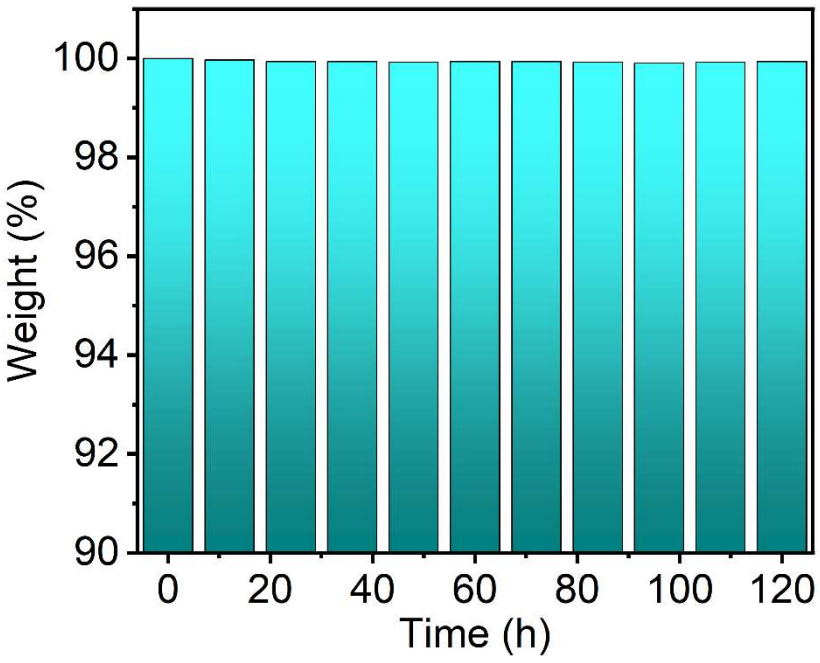

Supplementary Fig. 8 Simulated abrasion test of Al(fum)@5%Kaolin.

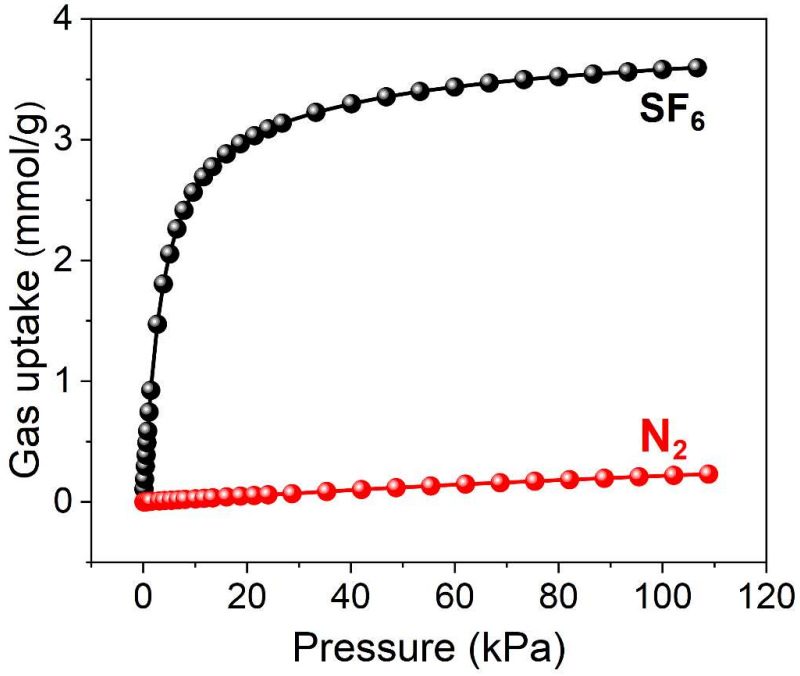

Supplementary Fig. 9 The SF_6 and N_2 isotherms on Al(fum) at 315 K.

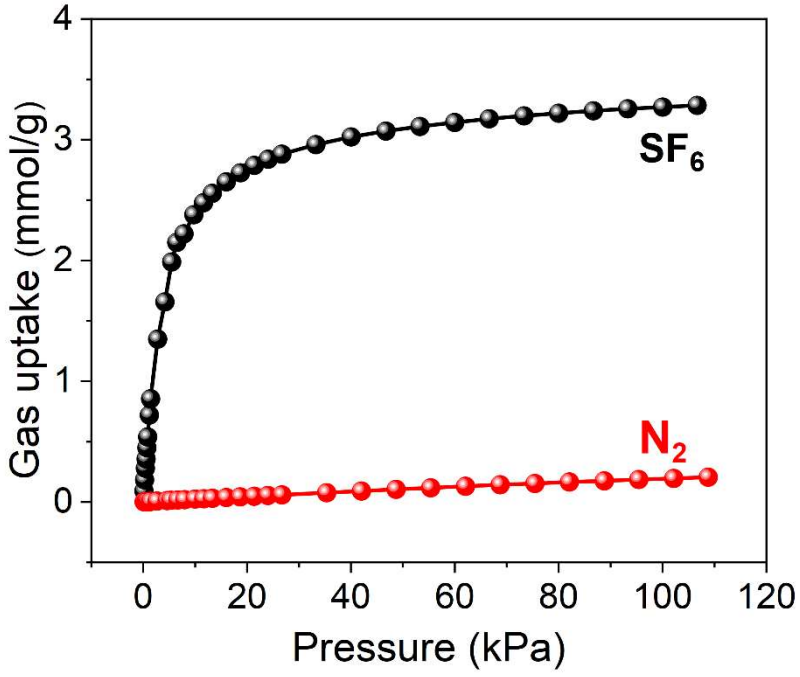

Supplementary Fig. 10 The SF_6 and N_2 isotherms on Al(fum)@2%HPC at 315 K.

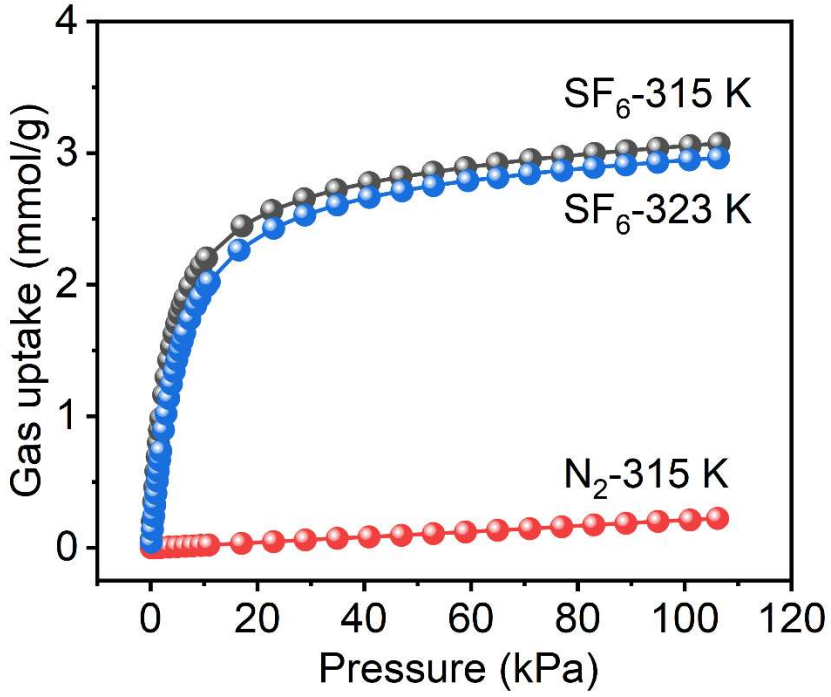

Supplementary Fig. 11 The SF_6 and N_2 isotherms on Al(fum)@5%Kaolin at 315 K and 323 K.

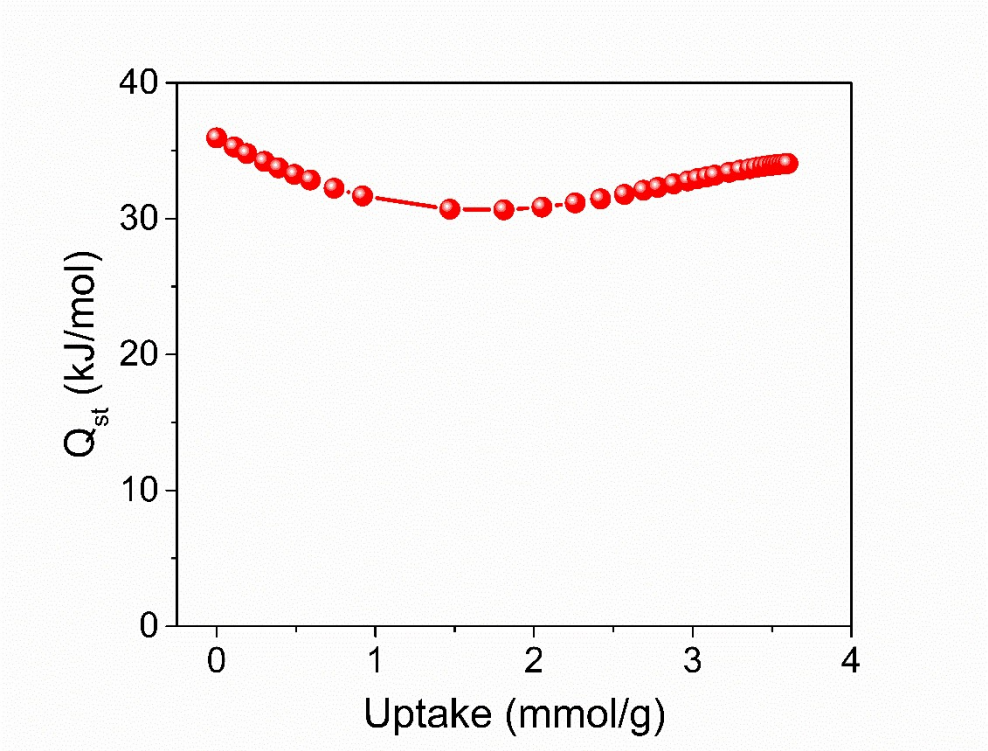

Supplementary Fig. 12 The isosteric heat of adsorption determined from Virial equations of SF_6 adsorption data for Al(fum).

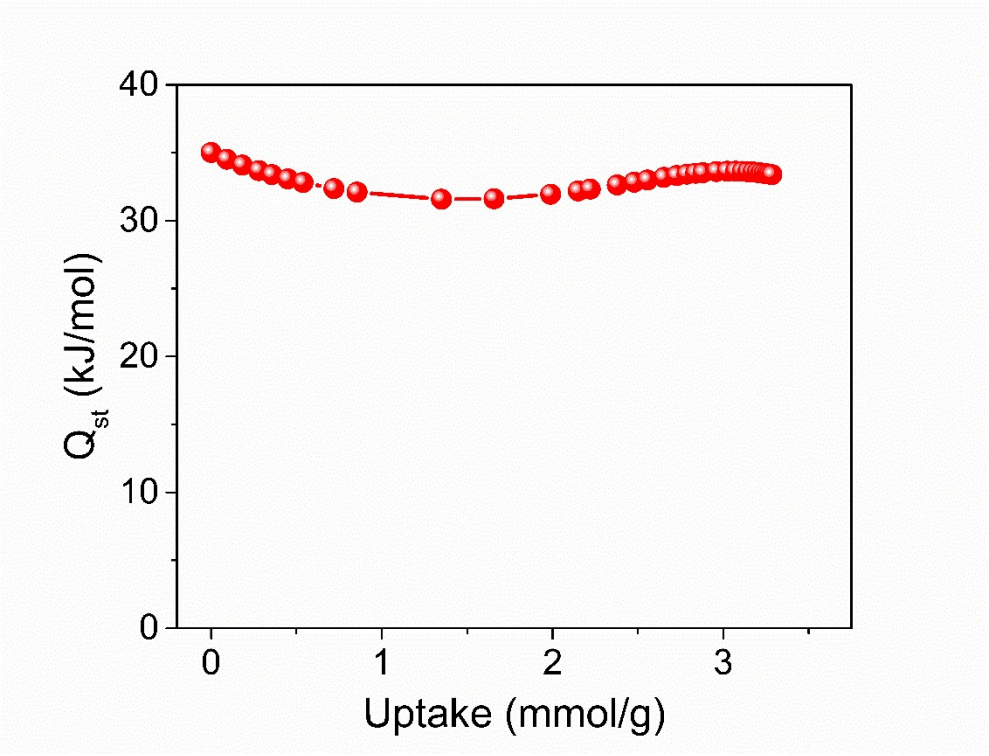

Supplementary Fig. 13 The isosteric heat of adsorption determined from Virial equations of SF_6 adsorption data for Al(fum)@2%HPC.

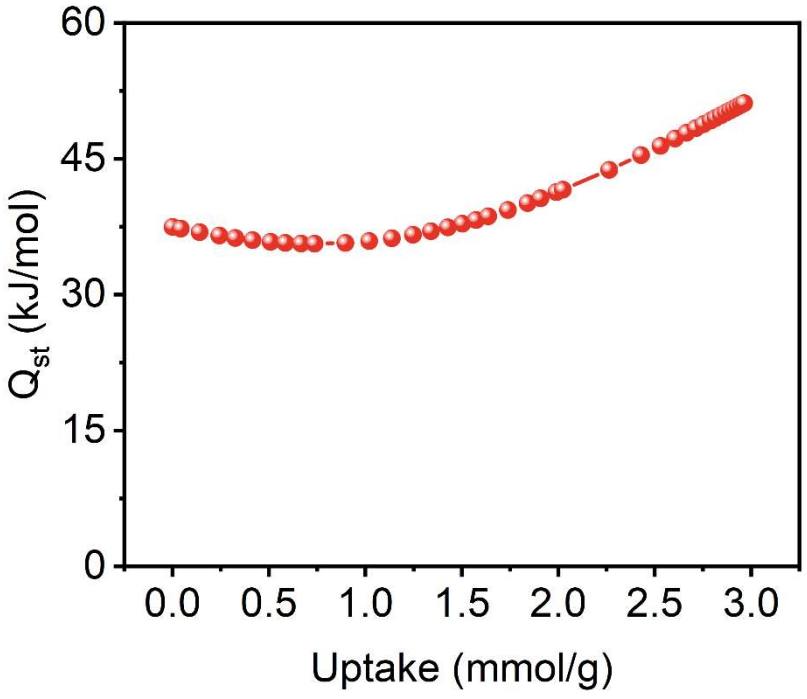

Supplementary Fig. 14 The isosteric heat of adsorption determined from Virial equations of SF_6 adsorption data for Al(fum)@5%Kaolin.

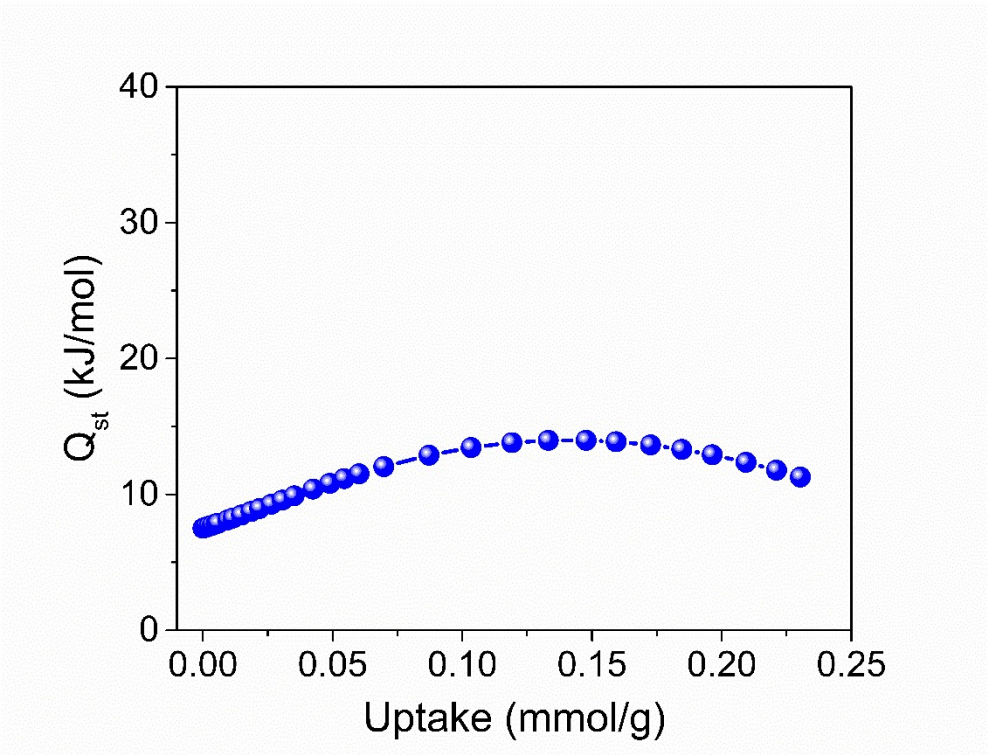

Supplementary Fig. 15 The isosteric heat of adsorption determined from Virial equations of N_2 adsorption data for Al(fum).

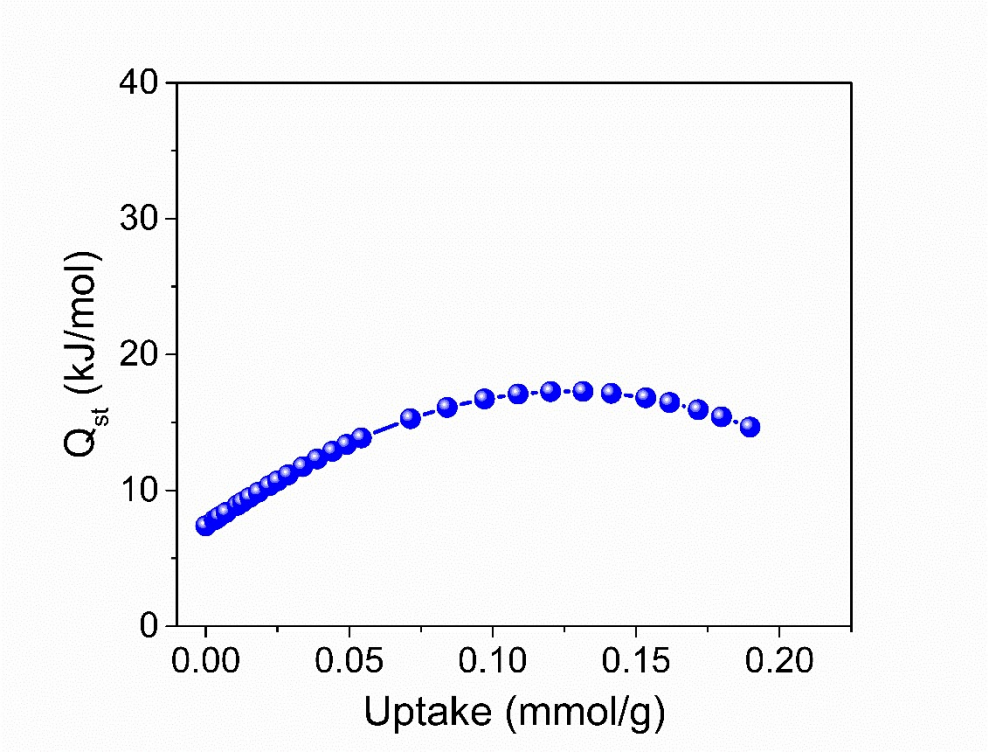

Supplementary Fig. 16 The isosteric heat of adsorption determined from Virial equations of N_2 adsorption data for Al(fum)@2%HPC.

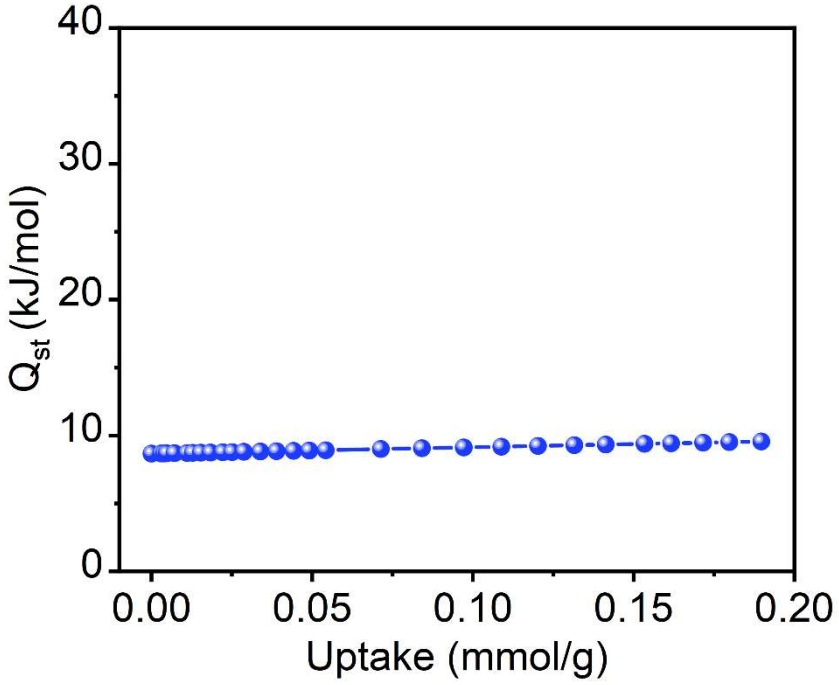

Supplementary Fig. 17 The isosteric heat of adsorption determined from Virial equations of N_2 adsorption data for Al(fum)@5%Kaolin.

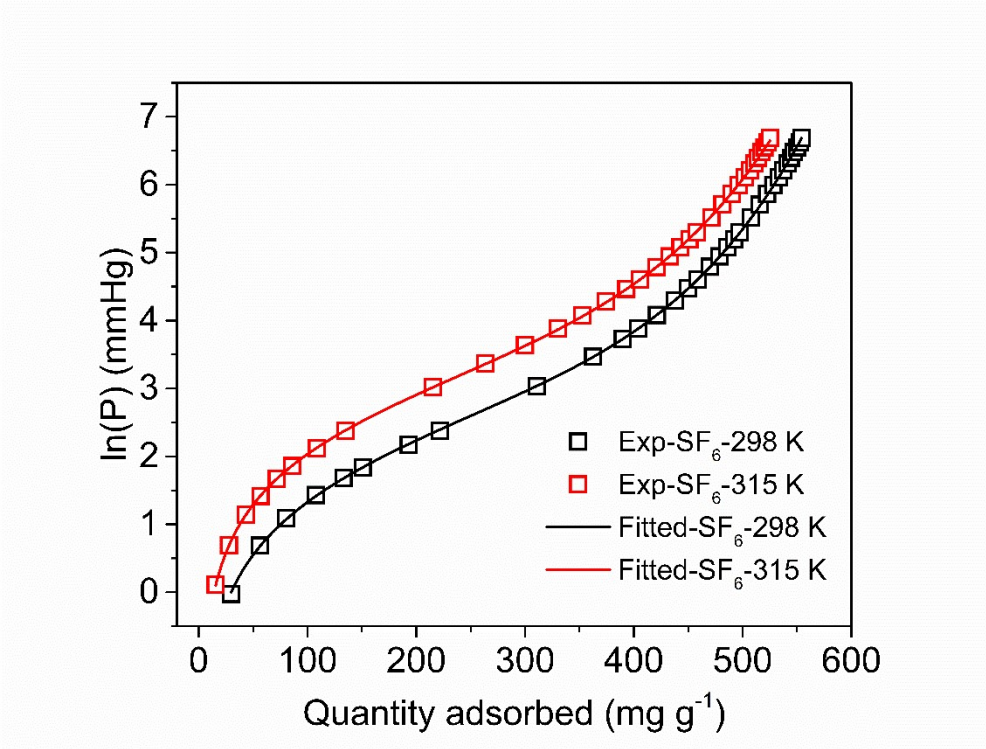

Supplementary Fig. 18 The Virial fitting of SF_6 adsorption data for Al(fum).

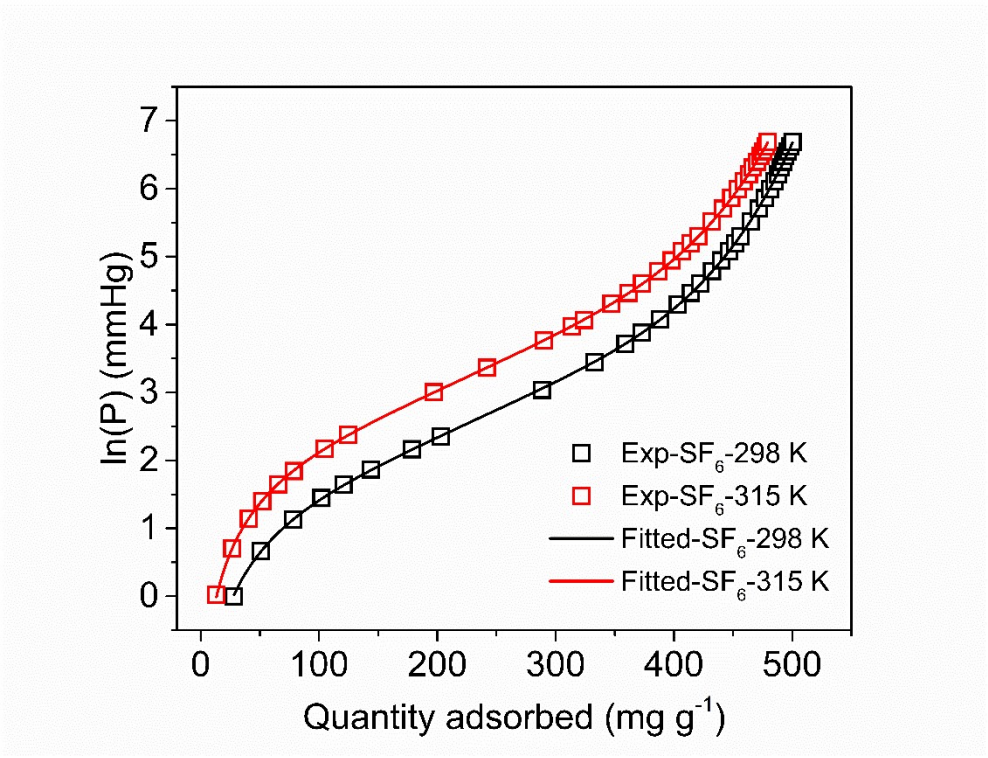

Supplementary Fig. 19 The Virial fitting of SF_6 adsorption data for Al(fum)@2%HPC.

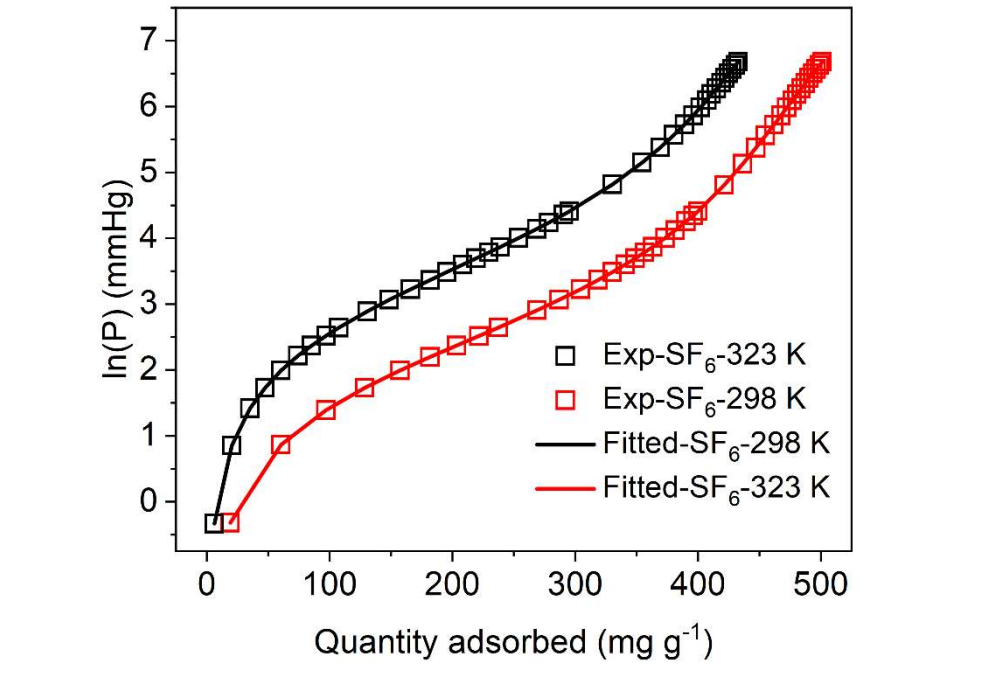

Supplementary Fig. 20 The Virial fitting of SF_6 adsorption data for Al(fum)@5%Kaolin.

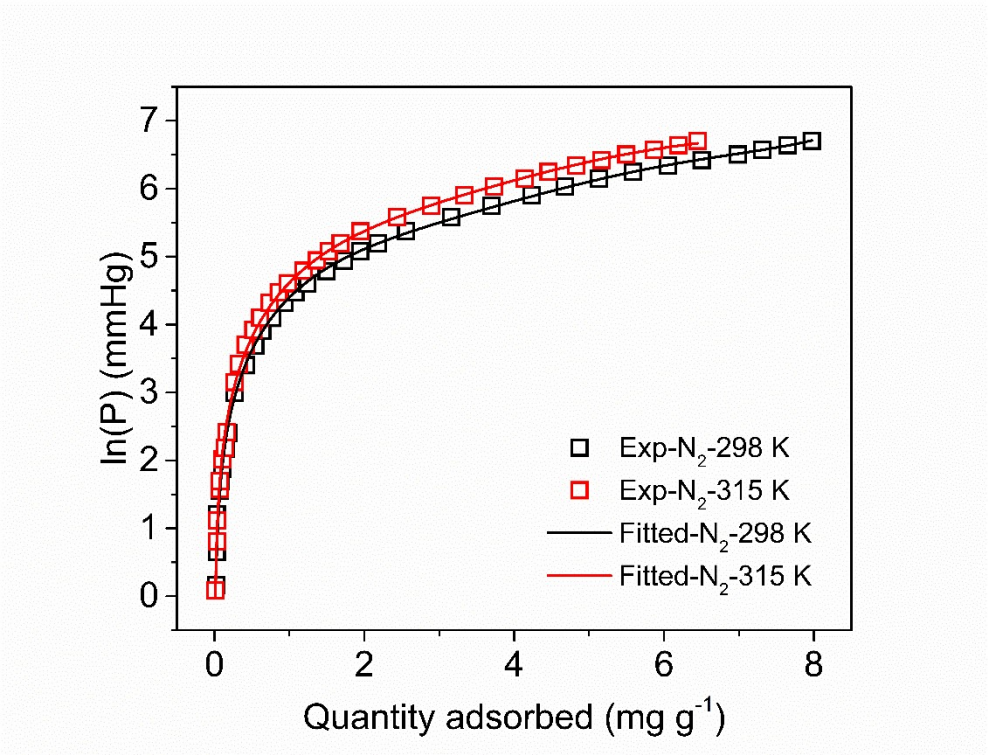

Supplementary Fig. 21 The Virial fitting of N_2 adsorption data for Al(fum).

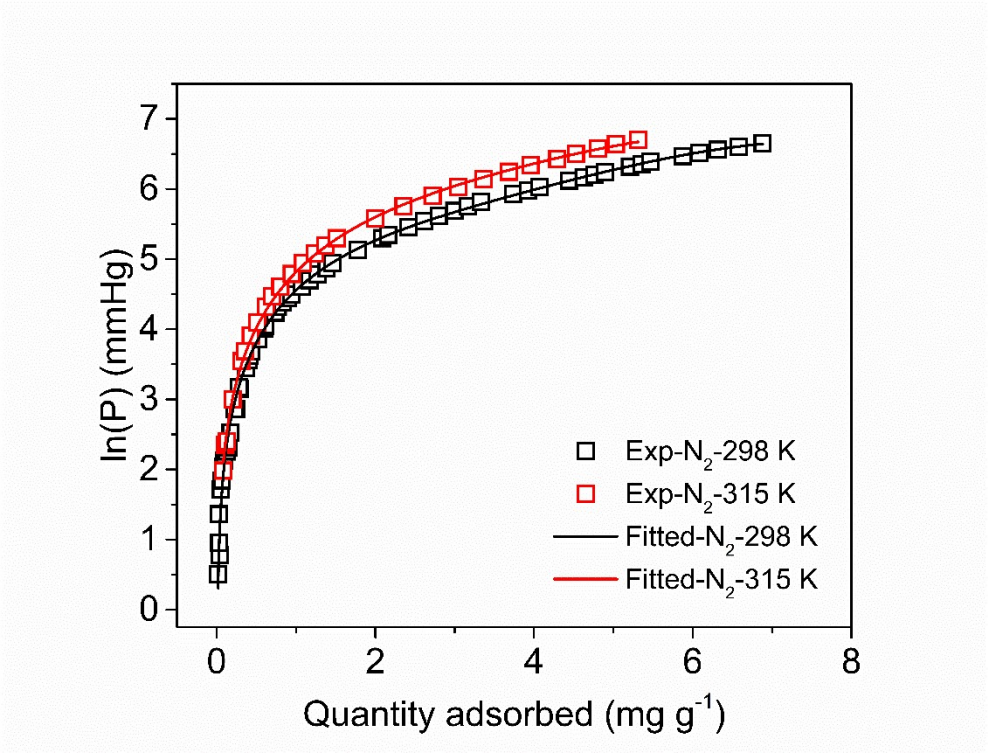

Supplementary Fig. 22 The Virial fitting of N_2 adsorption data for Al(fum)@2%HPC.

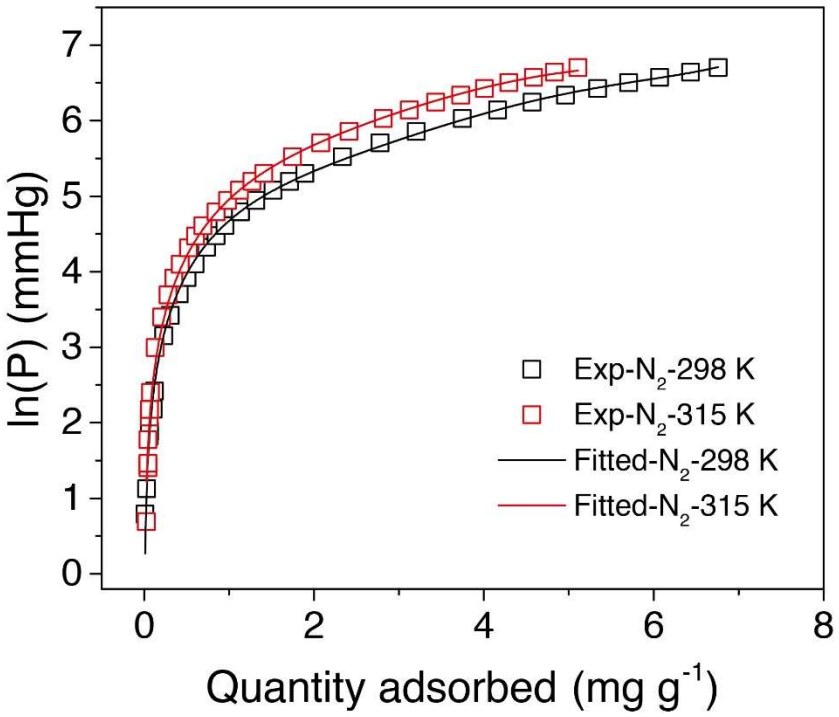

Supplementary Fig. 23 The Virial fitting of N_2 adsorption data for Al(fum)@5%Kaolin.

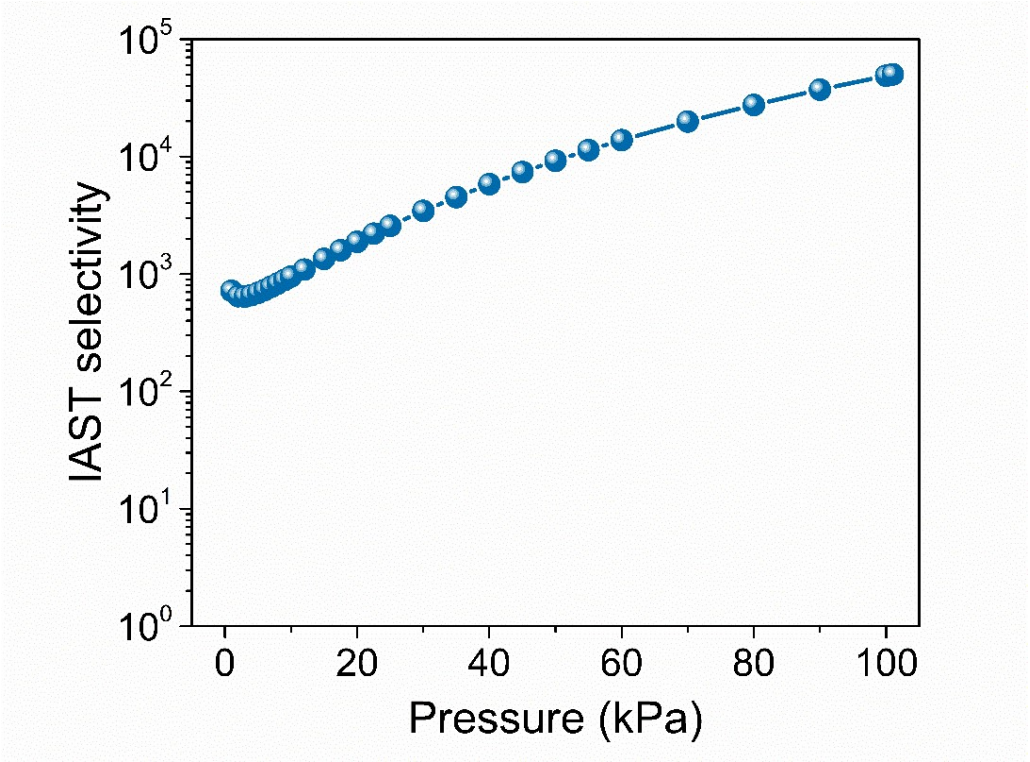

Supplementary Fig. 24 The IAST selectivities of SF_6/N_2 mixture (10/90, *v/v*) for Al(fum) at 298 K up to 1 bar.

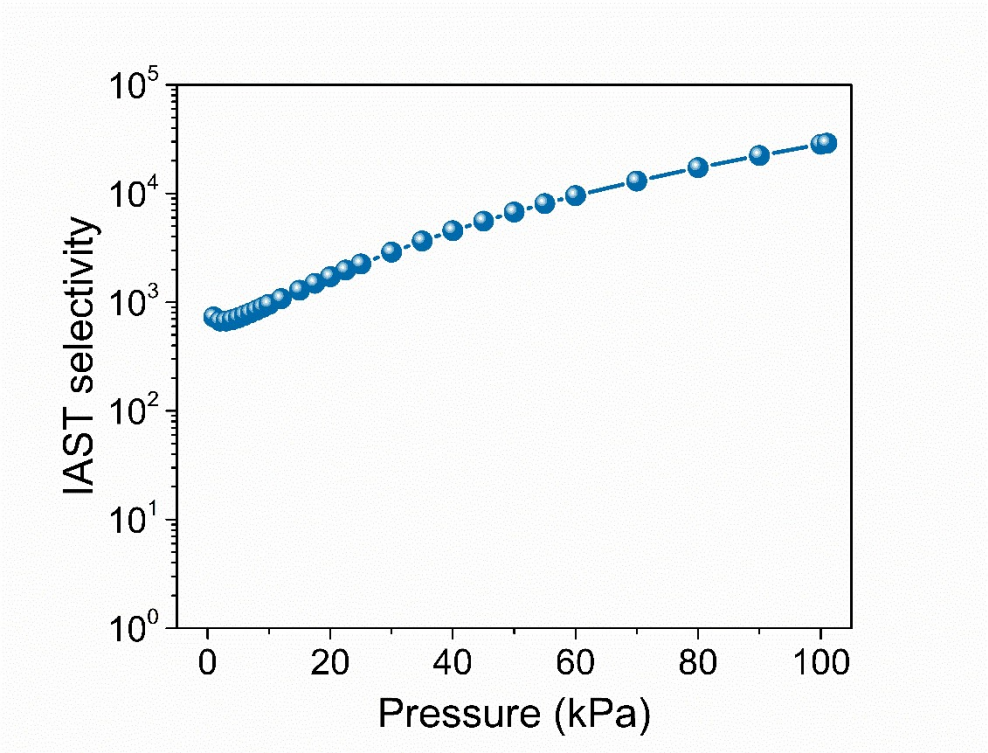

Supplementary Fig. 25 The IAST selectivities of SF_6/N_2 (10/90, *v/v*) mixture for Al(fum)@2%HPC at 298 K up to 1 bar.

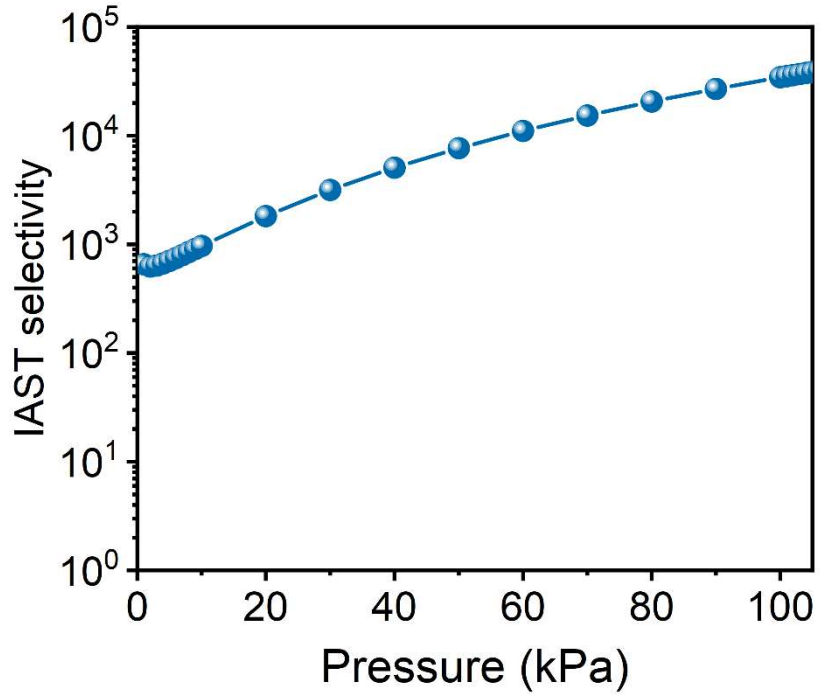

Supplementary Fig. 26 The IAST selectivities of SF_6/N_2 (10/90, *v/v*) mixture for Al(fum)@5%Kaolin at 298 K up to 1 bar.

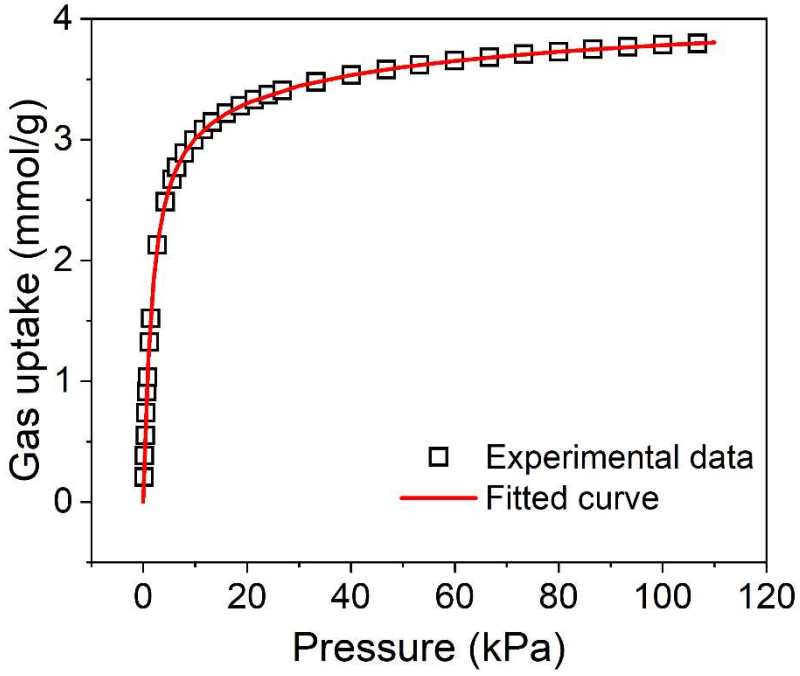

Supplementary Fig. 27 DSLF fitting of the SF_6 adsorption data at 298 K for Al(fum).

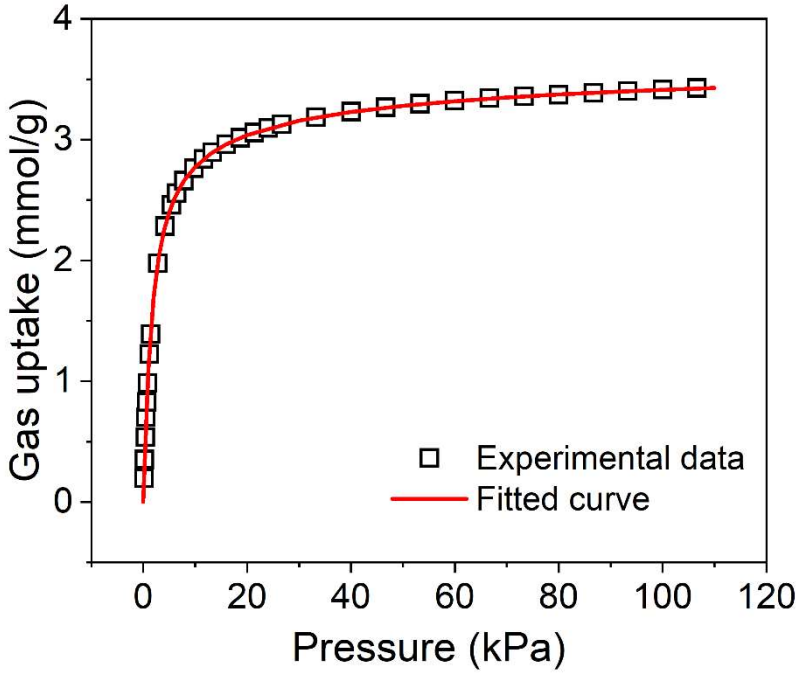

Supplementary Fig. 28 DSLF fitting of the SF_6 adsorption data at 298 K for Al(fum)@2%HPC.

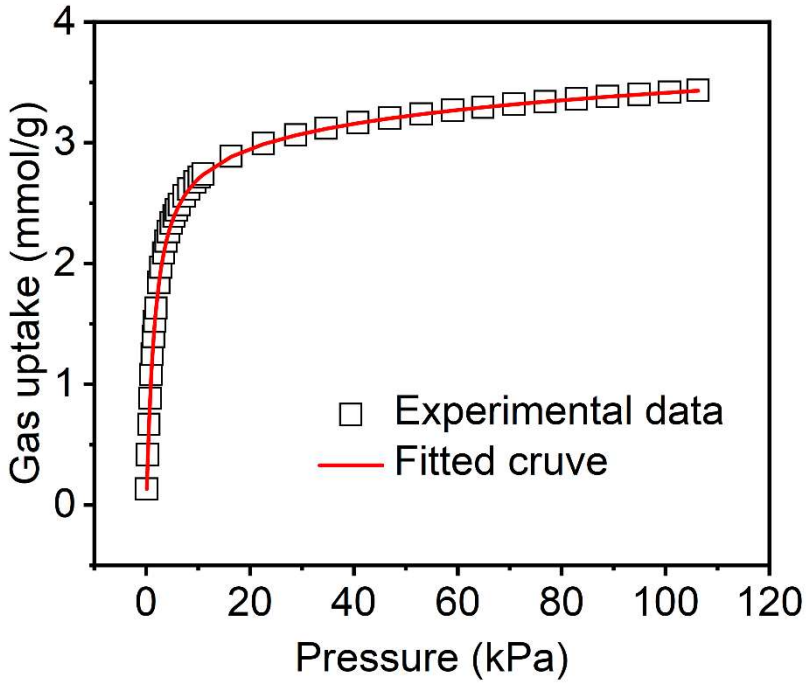

Supplementary Fig. 29 DSLF fitting of the SF_6 adsorption data at 298 K for Al(fum)@5%Kaolin.

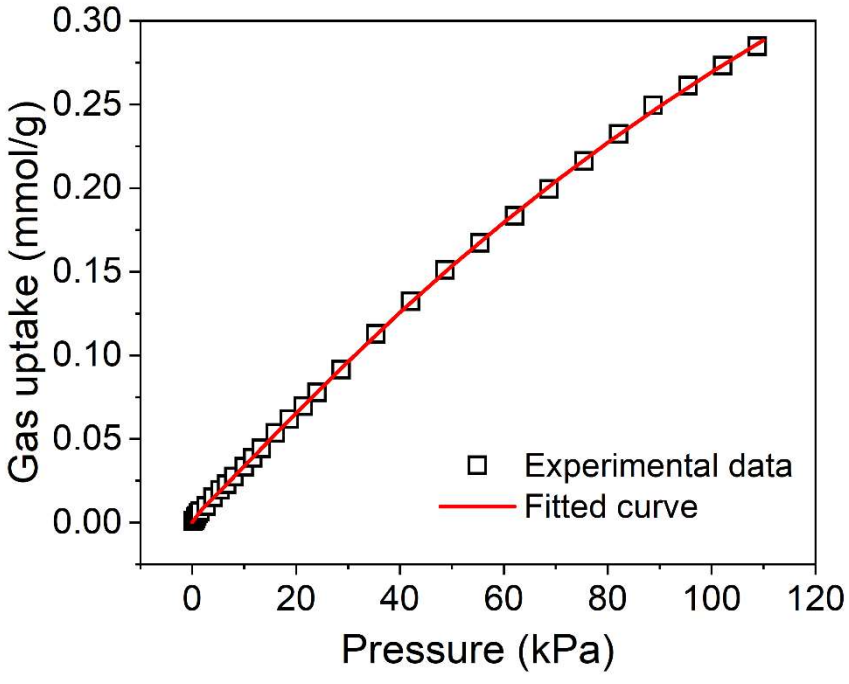

Supplementary Fig. 30 DSLF fitting of the N_2 adsorption data at 298 K for Al(fum).

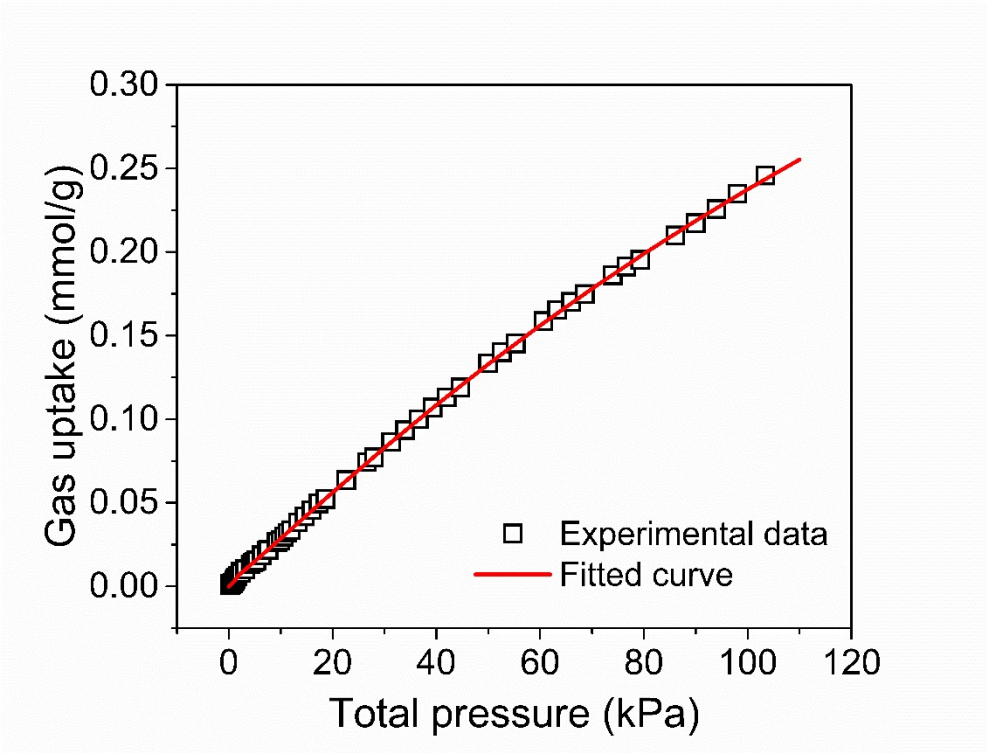

81

82 **Supplementary Fig. 31** DSLF fitting of the N_2 adsorption data at 298 K for Al(fum)@2%HPC.

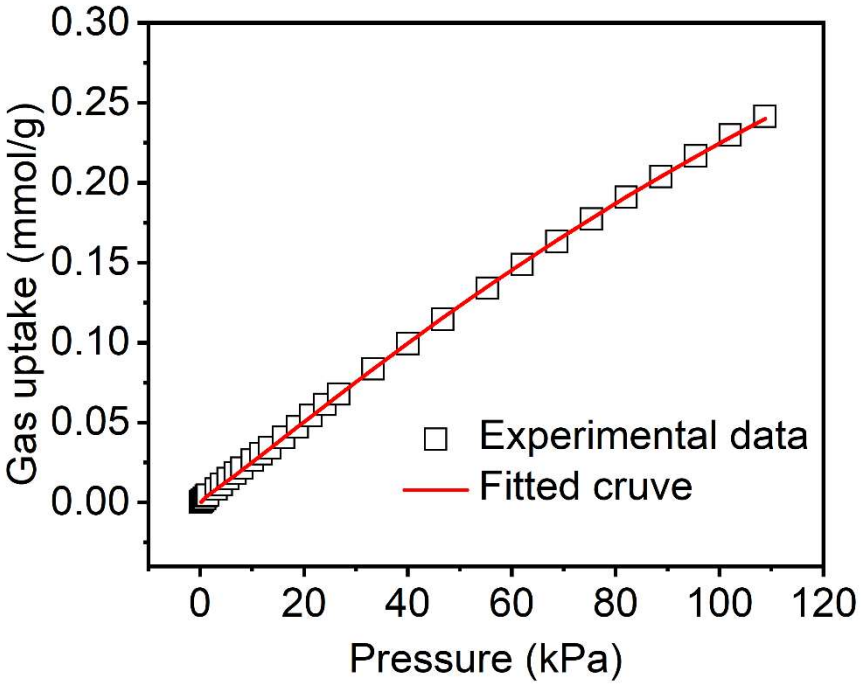

83

84 **Supplementary Fig. 32** DSLF fitting of the N_2 adsorption data at 298 K for Al(fum)@5%Kaolin.

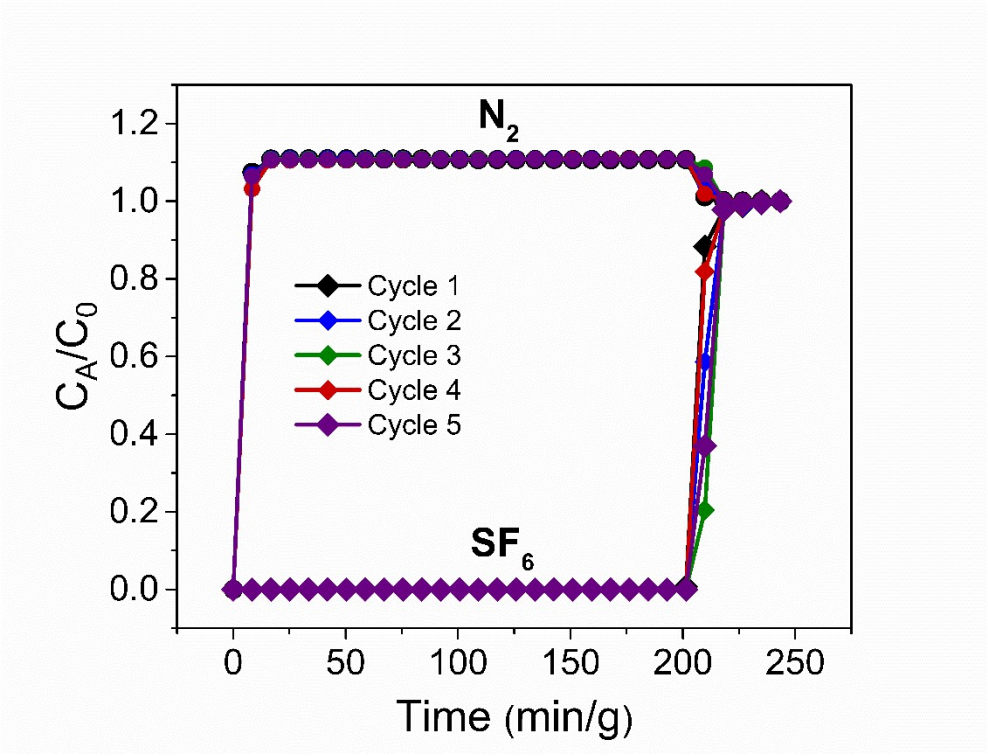

Supplementary Fig. 33 Cycling column breakthrough curves for SF_6/N_2 mixture (10/90, *v/v*) for Al(fum) at 298 K.

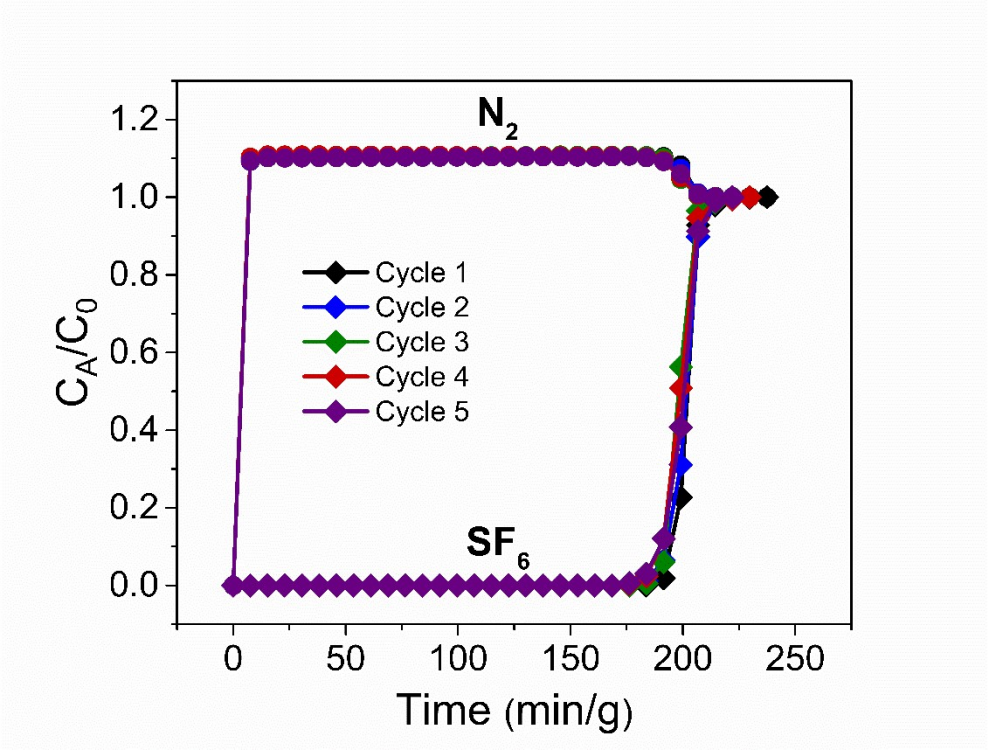

Supplementary Fig. 34 Cycling column breakthrough curves for SF_6/N_2 mixture (10/90, *v/v*) for Al(fum)@2%HPC at 298 K.

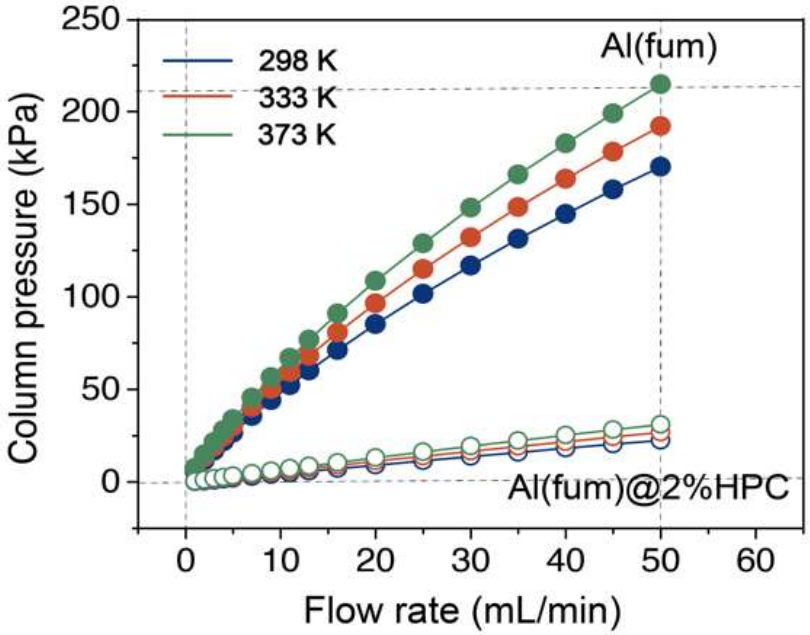

91

92 **Supplementary Fig. 35** Bed pressure drop values of Al(fum) and Al(fum)@2%HPC.

93

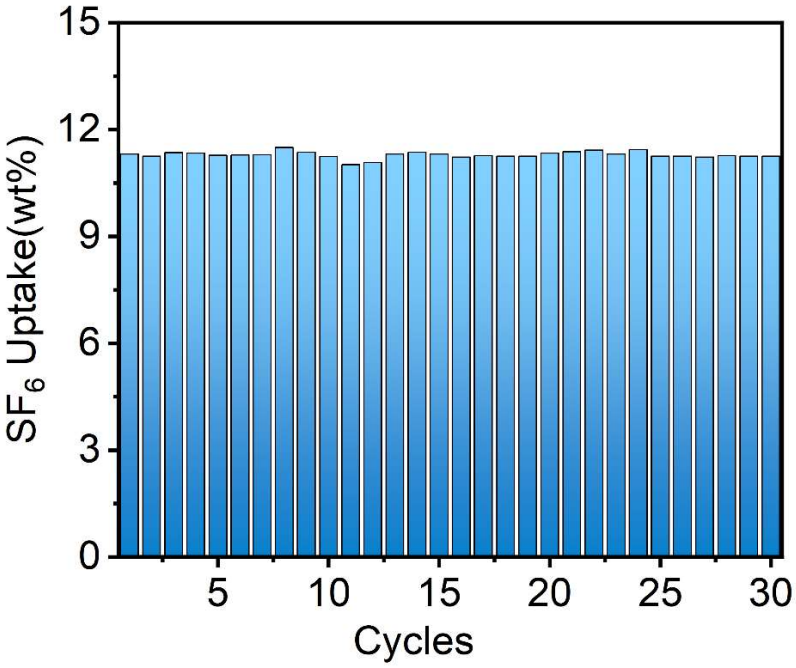

94

95 **Supplementary Fig. 36** SF_6 breakthrough for 30 cycles at 303K (adsorption) and 333 K (desorption).

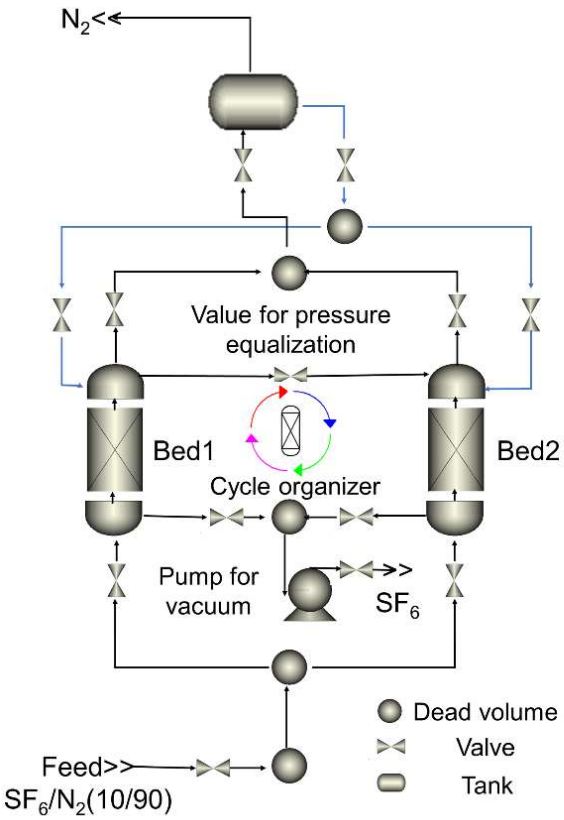

Supplementary Fig. 37 Schematic model of single-stage VTSA process.

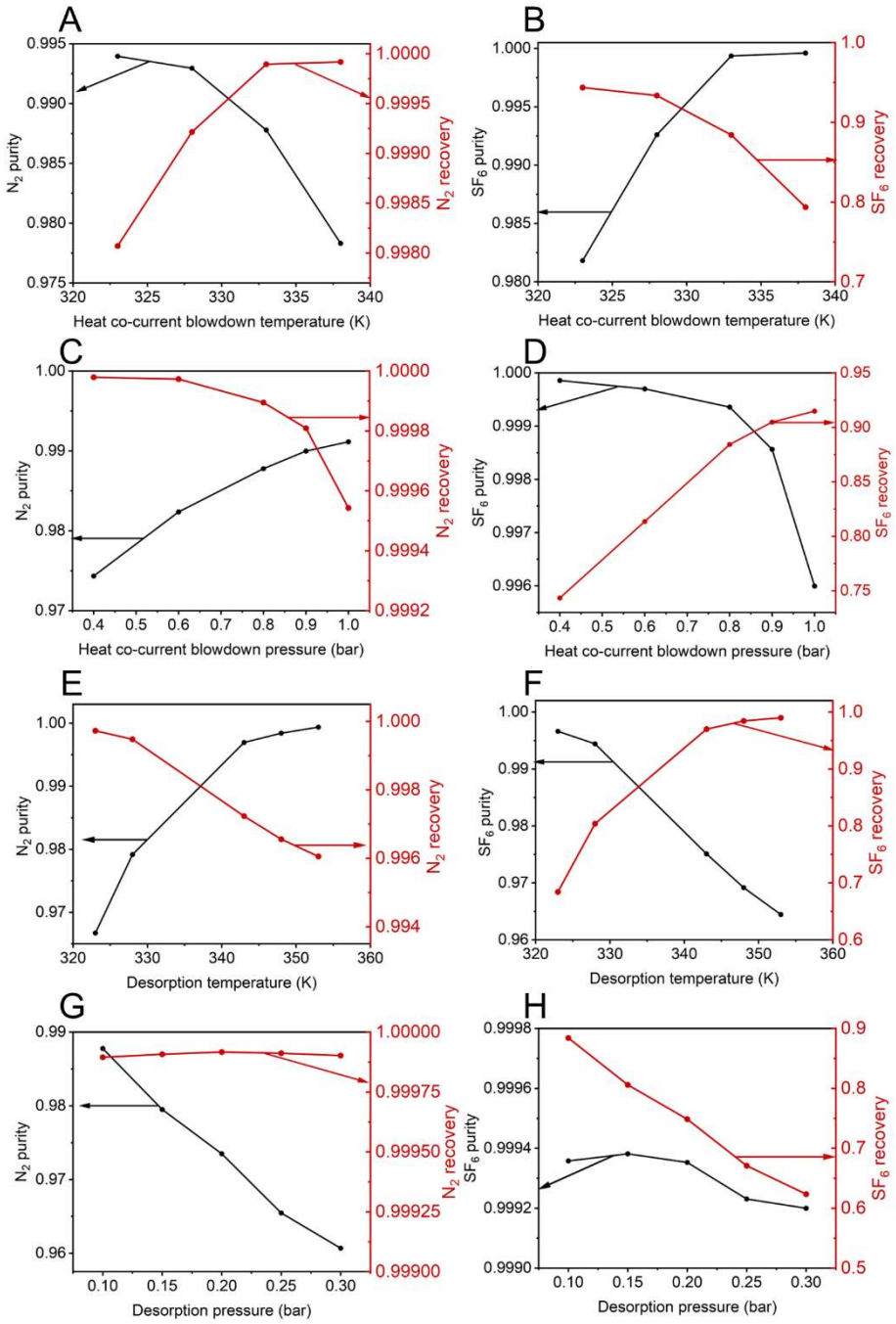

98

99 **Supplementary Fig. 38** Influence of single-stage VTSA parameters on purity and recovery. (**A**, **B**),

100 Heating co-current blowdown temperature, P_H=1.5 bar, P_L=0.1 bar, P_{PP}=0.8 bar, T_H=338 K. (**C**, **D**),

101 Heating co-current blowdown pressure, P_H=1.5 bar, P_L=0.1 bar, T_H=338 K, T_{PP}=333 K. (**E, F**),

102 Desorption temperature, P_H=1.5 bar, P_{PP}=0.8 bar, P_L=0.1 bar, T_H=338 K. (**G**, **H**), Desorption pressure,

103 P_H=1.5 bar, P_{PP}=0.8 bar, T_H=338 K, T_{PP}=333 K.

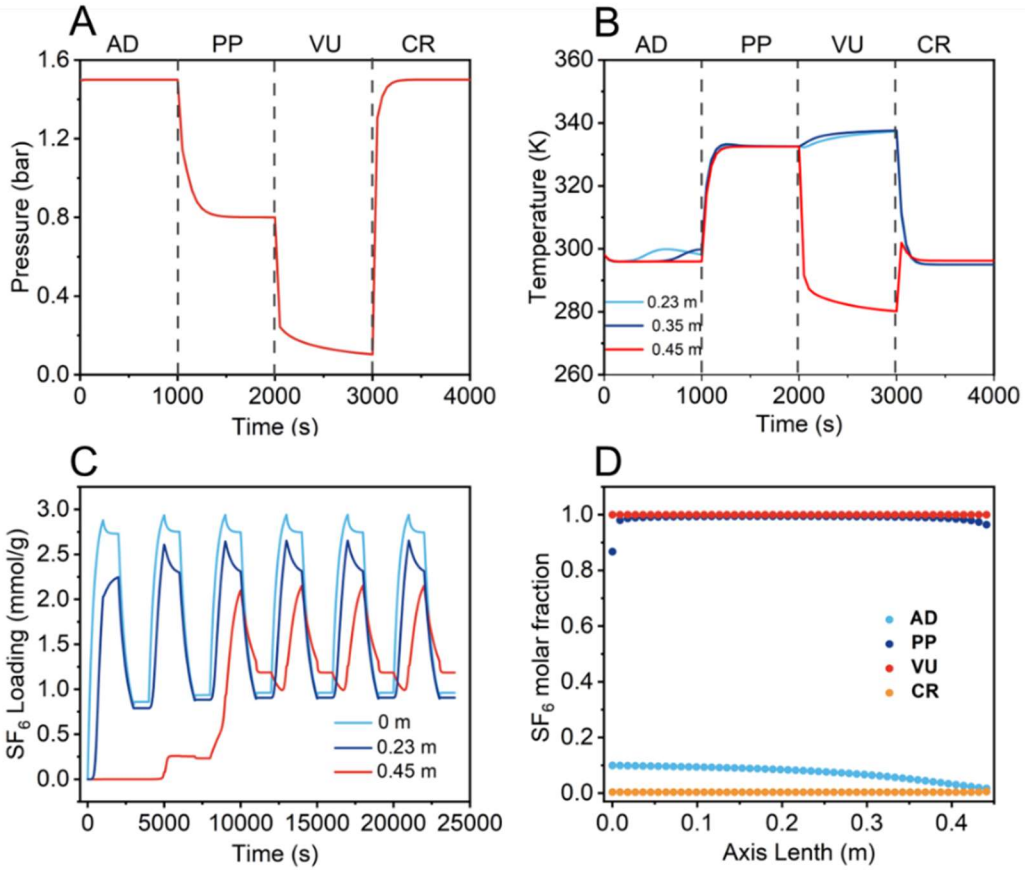

Supplementary Fig. 39 (**A**), Pressure profiles. (**B**), Temperature profiles. (**C**), SF_6 loading profiles on the Al(fum)@5%Kaolin. (**D**), SF_6 gas phase concentration profiles in the column for single-stage VTSA.

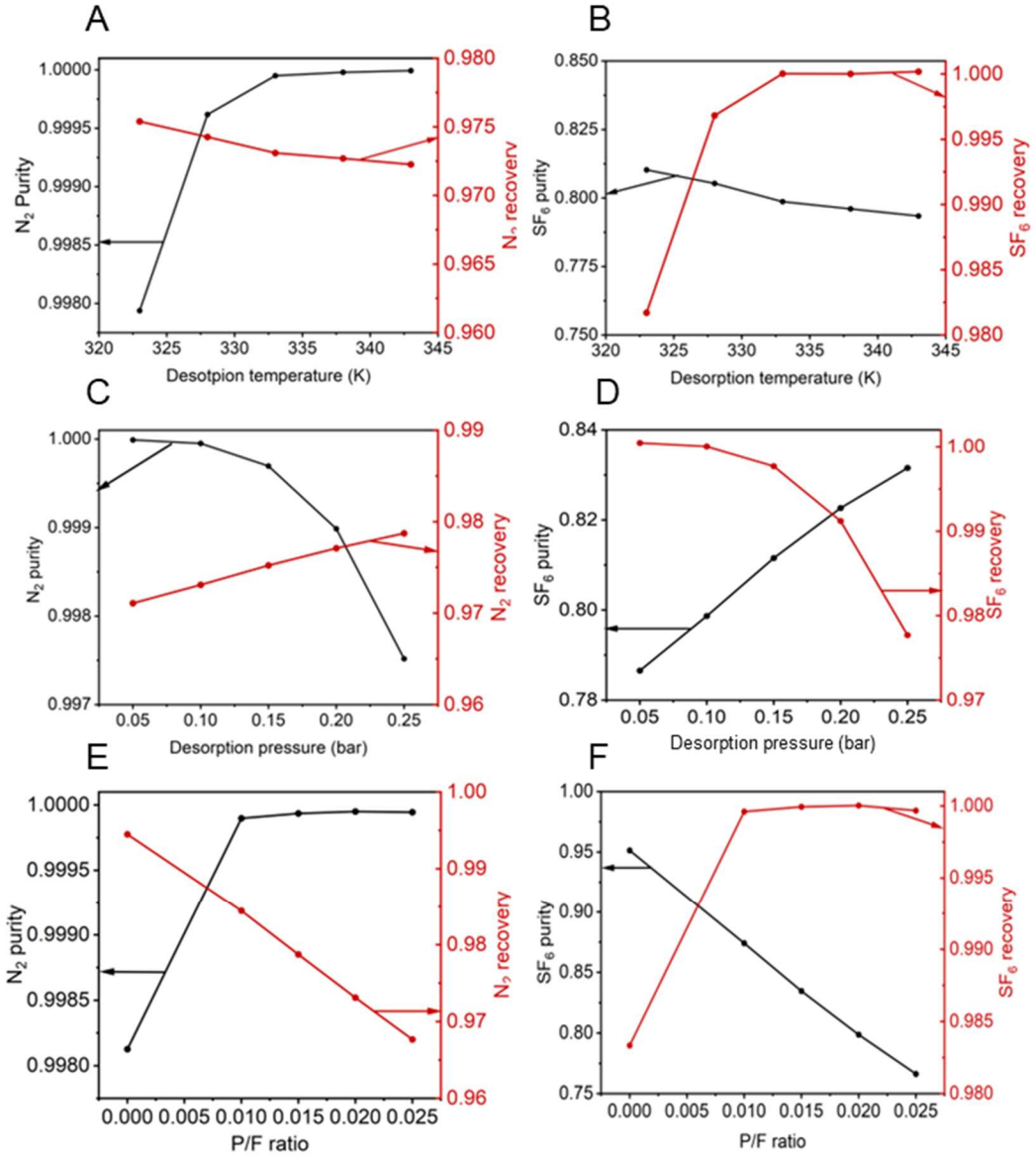

Supplementary Fig. 40 Influence of first-stage VTSA parameters on purity and recovery. (**A**, **B**), Desorption temperature, P_H=1.5 bar, P_L=0.1 bar, P/F ratio=0.02. (**C**, **D**), Desorption pressure, P_H=1.5 bar, T_H=333 K, P/F ratio=0.02. (**E**, **F**), P/F ratio, P_H=1.5 bar, P_L=0.1 bar, T_H=333 K.

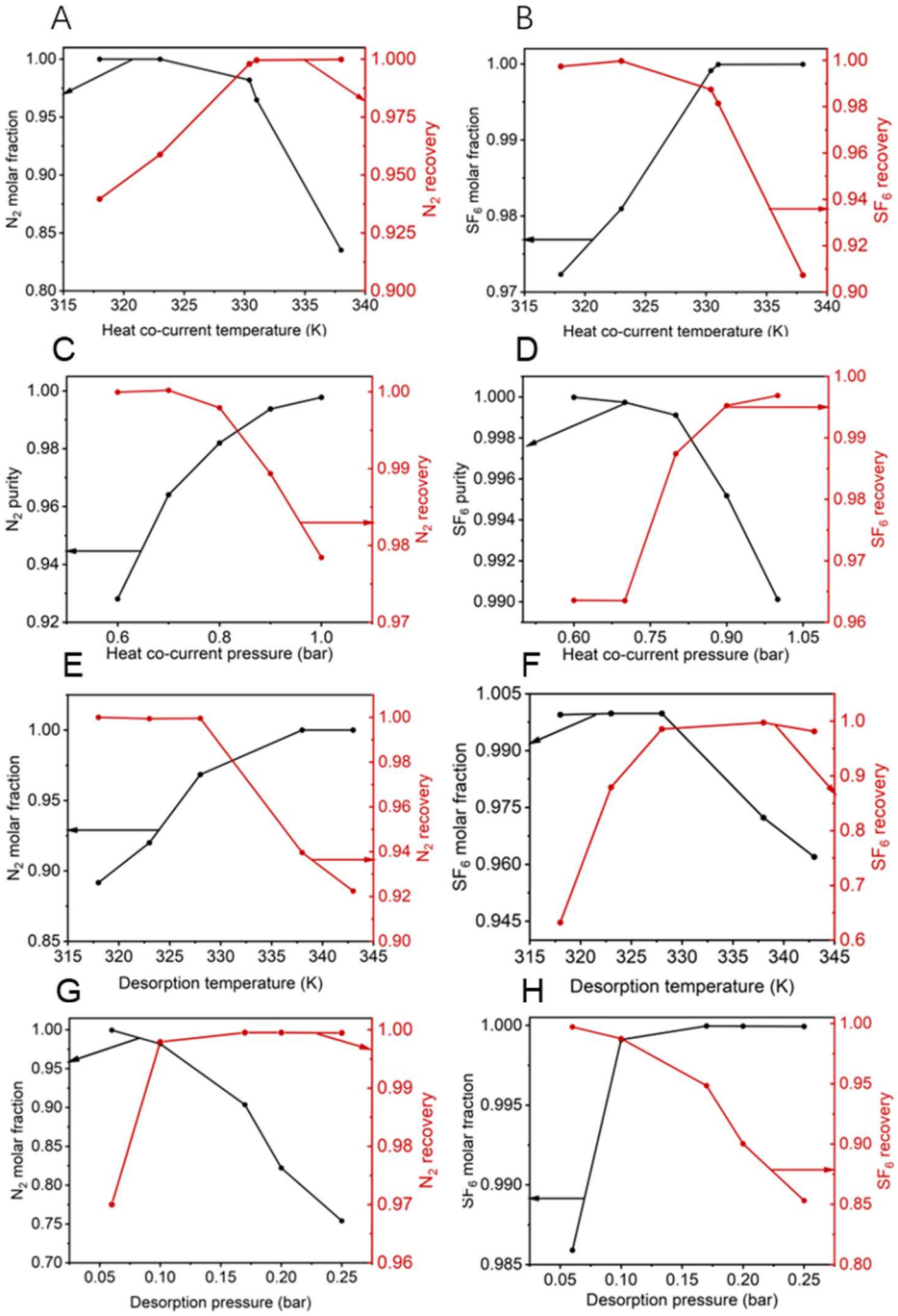

111

112 **Supplementary Fig. 41** Influence of two-stage VTSA parameters on purity and recovery. (**A**, **B**),

113 Heating co-current temperature, P_H=1.5 bar, P_L=0.1 bar, P_{PP}=0.8 bar, T_H=333 K. (**C**, **D**), Heating co-

114 current pressure, P_H=1.5 bar, P_L=0.1 bar, T_H=333 K, T_{PP}=328 K. (**E**, **F**), Desorption temperature, P_H=1.5

115 bar, P_{PP}=0.8 bar, P_L=0.1 bar, T_{PP}=333 K. (**G**, **H**), Desorption pressure, P_H=1.5 bar, P_{PP}=0.8 bar, T_H=333

116 K, T_{PP}=328 K.

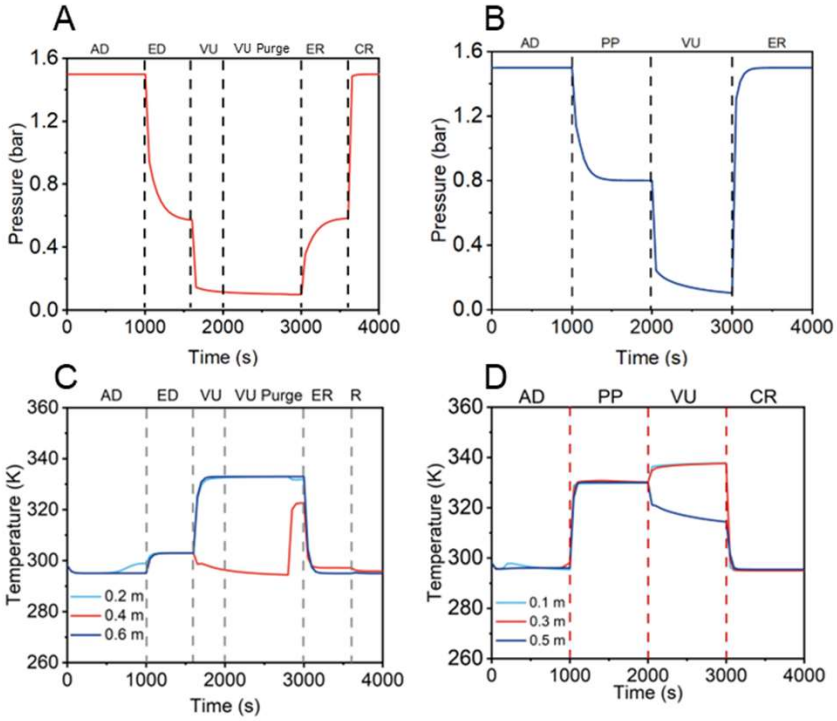

Supplementary Fig. 42 Pressure profiles of VTSA over on cycle (**A**), the first stage. (**B**), The second stage. Temperature profiles of VTSA over on cycle (**C**), the first stage. (**D**), The second stage.

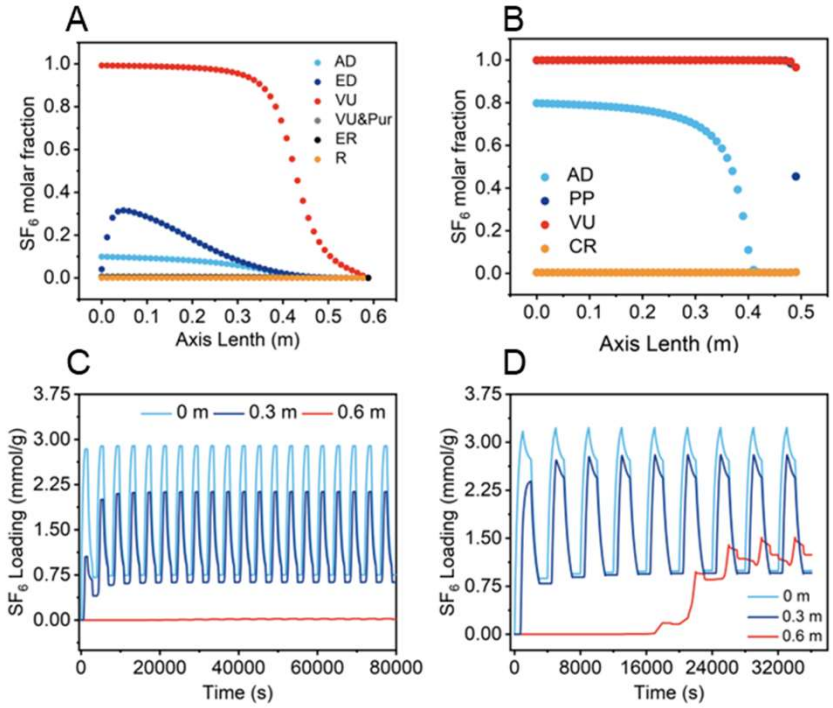

Supplementary Fig. 43 The second stage. SF_6 loading profiles of VTSA over on cycle (**A**), The first stage. (**B**), The second stage.SF_6 gas phase concentration profiles for two-stage VTSA (**C**), The first stage (**D**), The second stage.

Supplementary Table 1. DSLF fitting parameters for SF_6 and N_2 in Al(fum) at 298 K.

Gas	Site A			Site B			R^2
	$q_{A,sat}$ mmol/g	b_A kPa^{-1}	v_A	$q_{B,sat}$ mmol/g	b_B kPa^{-1}	v_B	
SF_6	1.92453	0.18170	0.54749	2.45960	0.56538	1.29267	0.99999
N_2	0.00341	1.35281	2.70231	0.82352	0.00305	1.09730	0.99991

Supplementary Table 2. DSLF fitting parameters for SF_6 and N_2 in Al(fum)@2%HPC at 298 K.

Gas	Site A			Site B			R^2
	$q_{A,sat}$ mmol/g	b_A kPa^{-1}	v_A	$q_{B,sat}$ mmol/g	b_B kPa^{-1}	v_B	
SF_6	1.55684	0.24634	0.60875	2.17274	0.57610	1.29147	0.99999
N_2	0.00228	0.40065	8.18894	0.84424	0.00271	1.07682	0.99991

Supplementary Table 3. DSLF fitting parameters for SF_6 and N_2 in Al(fum)@5%Kaolin at 298 K.

Gas	Site A			Site B			R^2
	$q_{A,sat}$ mmol/g	b_A kPa^{-1}	v_A	$q_{B,sat}$ mmol/g	b_B kPa^{-1}	v_B	
SF_6	2.09380	0.06819	0.50870	2.56050	0.60488	1.20607	0.99999
N_2	0.00200	1.46820	3.04537	0.80035	0.00230	1.11233	0.99982

Supplementary Table 4. Isotherm parameters for SF_6 and N_2 on Al(fum)@5%Kaolin by regression.

Parameter	Al(fum)@5%Kaolin	
	N_2	SF_6
IP_1 / kmol/(kg bar)	3.79×10^{-5}	1.81×10^{-13}
IP_2 / K	566	8260
IP_3 / bar^{-1}	8.56×10^{-5}	1.46×10^{-10}
IP_4 / K	2112	7961
R^2	0.999	0.995

Supplementary Table 5. The adsorption bed parameters of single-stage VTSA.

Parameter	Description	Value
W_t / m	Wall thickness used of bed	0.0005
H_b / m	Height of adsorbent layer	0.45
D_b / m	Internal diameter of adsorbent layer	0.15
E_i / m^3/m^3	Inter-particle voidage	0.4
E_p / m^3/m^3	Intra-particle voidage	0.205
RHO_s / m^3/m^3	Bulk solid density of adsorbent	405
R_p / mm	Adsorbent particle radius	1.5
SFac	Adsorbent shape factor	0.78
MTC (N_2)/s^{-1}	Constant mass transfer coefficients	0.0232
MTC (SF_6)/s^{-1}	Constant mass transfer coefficients	0.00288
C_{ps} / MJ /(kg K)	Adsorbent specific heat capacity	0.00119
DH(N_2) / MJ/kmol	Constant for heat of adsorption	-8.7
DH(SF_6) / MJ/kmol	Constant for heat of adsorption	-37.5
HTC / MW/(m^2 K)	Constant for the heat transfer coefficient	0.76
K_g / MW/(m^2 K)	Constant for the gas phase heat conductivity	2.35×10^{-7}
K_s / MW/(m^2 K)	Adsorbent thermal conductivity	1×10^{-6}

Supplementary Table 6. The adsorption bed parameters of two-stage VTSA.

Parameter	Description	Value	
		first-stage VTSA	second-stage VTSA
H_b / m	Height of adsorbent layer	0.60	0.50
D_b / m	Internal diameter of adsorbent layer	0.15	0.15

Supplementary Table 7. Optimized parameter of Single stage and Two stage VTSA.

	Single stage VTSA	Two stage VTSA	
		first-stage VTSA	second-stage VTSA
Heating co-current pressure/ bar	0.8	-	0.8
Heating co-current temperature/ K	333	-	328
Desorption pressure/ bar	0.1	0.1	0.1
Desorption temperature/ K	338	333	333
Purge to feed ratio (P/F ratio)	-	0.02	-

133 **Supplementary Table 8.** The optimized parameters of cryogenic distillation simulation.

		Feedstock	Top of distillation column	Bottom of distillation column
Mass flow rate /kg/h		3.084	1.953	1.131
Mole flow rate /kmol/h		0.077	0.070	0.007
Temperature /K		93	104	264
pressure /bar		10	10	10
Component mass flow rate /kg/h				
SF_6		1.95	0	1.13
N_2		1.13	1.95	0
Component mole flowrate /kmol/h				
SF_6		0.008	0	0.008
N_2		0.070	0.070	0
Component mole fraction				
SF_6		0.1	0	0.999
N_2		0.9	1	0.001
Overall energy consumption	heat	1.64	0.36	0.53
/ MJ/kg SF_6	pump	0.75	-	-
SF_6 energy consumption / MJ/kg SF_6			1.76	

134

Supplementary Table 9. Comparison of the SF_6 uptake at 10 kPa, IAST predicted SF_6/N_2 (10/90) selectivities, the adsorption isosteric heat values (Q_{st}) of SF_6 and N_2 and Q_{st} ratio of SF_6/N_2 among different MOFs.

Adsorbents	SF_6 uptake	IAST selectivity	Q_{st} / kJ/mol			Ref
	mmol/g		SF_6	N_2	Ratio	
Al(fum)	**3.00**	**50139**	**35.9**	**7.5**	**4.79**	**This work**
Al(fum)@2%HPC	**2.79**	**28978**	**35.0**	**7.4**	**4.73**	
Al(fum)@5%Kaolin	**2.80**	**34409**	**37.5**	**8.7**	**4.33**	
$Ni(adc)(dabco)_{0.5}$	2.23	948	47.6	19.4	2.45	1
$Ni(NDC)(TED)_{0.5}$	2.78	750	34.1	13.1	2.60	2
$Ni(ina)_2$	2.39	375.1	33.4	16.1	2.07	3
SBMOF-1	0.89	325	32.5	15	2.17	4
Cu-MOF-NH_2	3.39	266.2	55.2	19.1	2.89	5
C-PVDC-800	2.15	244.8	36.9	14.8	2.49	6
UiO-66-Br_2	0.75	220	44.3	-	-	7
$Ni(pba)_2$	1.7	200.6	24	16.7	1.44	3
UiO-66	0.82	127.8	32.1	-	-	7
$Ph_8M_2Cs_{11}$	2.69	76.1	23	-	-	8
HKUST-1c	1.37	50.1	9.5	-	-	9
Zeolite-13X	0.99	56.5	23	18	1.28	10
MOF-74(Zn)	1.35	46	25	-	-	11
MOF-74(Co)	2.06	34.6	40	-	-	11
MOF-74(Mg)	2.1	19	32	-	-	11
CC3	0.88	74	40	-	-	12
CAU-17[a]	1.15	31	-	-	-	13
MIL-100(Fe)	0.25	24.4	20.5	17	1.21	14
$Zn(TMBDC)(DABCO)_{0.5}$	2.48	239	45.2	24.6	1.84	15
HBU-21	0.4	184	24.5	-	-	16
CAU-10-Py	1.13	203.6	32.6	17.5	1.86	17
3D-TMTAPB-COF	2.23	335	33.5	14.8	2.26	18
ACK1	1.80	684	30.6	21.5	1.42	19
YTU-30	0.85	325	27	13.8	1.96	20
SNNU-204	0.61	49	21	16.4	1.28	21
PC-750	2.32	437	32.9	17.2	1.91	22
$Ni(3\text{-}mpba)_2$	1.79	221	32	13	2.46	23

[a]This data was obtained at 273 K.

Reference

1. Chang, M. *et al.* Metal-organic framework-based single-molecule SF_6 trap for record SF_6 capture. *Chem. Mater.* **34**, 9134-9143 (2022).
2. Yang, M., Chang, M., Yan, T. & Liu, D. A nickel-based metal-organic framework for efficient SF_6/N_2 separation with record SF_6 uptake and SF_6/N_2 selectivity. *Sep. Purif. Technol.* **295**, 121340 (2022).
3. Wang, S. *et al*. Pore-structure control in metal-organic frameworks (MOFs) for capture of the greenhouse gas SF_6 with record separation. *Angew. Chem. Int. Ed.* **61**, e202207066 (2022).
4. Wang, T. *et al.* Calcium-based metal-organic framework for efficient capture of sulfur hexafluoride at low concentrations, *Ind. Eng. Chem. Res*. **60**, 5976-5983 (2021).
5. Ren, J. *et al.* Computer-aided discovery of MOFs with calixarene-analogous microenvironment for exceptional SF_6 capture. *Chem. Mater.* **33**, 5108-5114 (2021).
6. Huang, X. *et al.* Separation of perfluorinated electron specialty gases on microporous carbon adsorbents with record selectivity. *Sep. Purif. Technol.* **292**, 121059 (2022).
7. Kim, M. *et al.* Highly selective adsorption of SF_6 over N_2 in a bromine-functionalized zirconium-based metal-organic framework. *Chem. Eng. J.* **339**, 223-229 (2018).
8. Yang, Y. *et al.* Sub-Ångström-level engineering of ultra microporous carbons for enhanced sulfur hexafluoride capture, *Carbon* **155**, 56-64 (2019).
9. Chuah, C., Goh, K. & Bae, T. Hierarchically structured HKUST-1 nanocrystals for enhanced SF_6 capture and recovery. *J. Phys. Chem. C.* **121**, 6748-6755 (2017).
10. Kim, M. *et. al.* High SF_6/N_2 selectivity in a hydrothermally stable zirconium-based metal-organic framework. *Chem. Eng. J.* **276**, 315-321 (2015).
11. Kim, M., Lee, S., Lee, C. & Bae, Y. High SF_6 selectivities and capacities in isostructural metal-organic frameworks with proper pore sizes and highly dense unsaturated metal sites. *Micropor. Mesopor. Mat.* **190**, 356-361 (2014).
12. Hasell, T. *et al.* Porous organic cages for sulfur hexafluoride separation. *J. Am. Chem. Soc.* **138**, 1653-1659 (2016).

13. Köppen, M. *et al.* Synthesis, transformation, catalysis, and gas sorption investigations on the bismuth metal-organic framework CAU-17. *Eur. J. Inorg. Chem.* **2018**, 3496-3503 (2018).
14. Kim, P. *et al.* Separation of SF_6 from SF_6/N_2 mixture using metal–organic framework MIL-100 (Fe) granule. *Chem. Eng. J.* **262**, 683-690 (2015).
15. Yan, L. *et al*. Methyl-functionalized flexible ultra-microporous MOF for efficient SF_6/N_2 mixture separation. *Chem. Eng. J.* **472**, 145145 (2023).
16. Yan, J. *et al.* An In(III)-MOF based on pore engineering for efficient capture SF_6 from SF_6/N_2 mixture. *Sep. Purif. Technol.* **327**, 124929 (2023).
17. Hu, Y. *et al*. Pore engineering in cost-effective and stable Al-MOFs for efficient capture of the greenhouse gas SF_6. *Chem. Eng. J.* **471**, 144851 (2023).
18. Yin, Y. *et al.* Single-crystal three-dimensional covalent organic framework constructed from 6-connected triangular prism node. *J. Am. Chem. Soc.* **145**, 22329-22334 (2023).
19. Wang, J. *et al.* Modulation of pore structure in a microporous carbon for enhanced adsorption of perfluorinated electron specialty gases with efficient separation. *Chem. Eng. J.* **477**, 147128 (2023).
20. Li, Y. *et al.* Design of a highly-stable cobalt (II) porous framework based on aromatic stacking strategy for efficient SF_6 capture and SF_6/N_2 mixture separation. *Sep. Purif. Technol.* **343**, 126995 (2024).
21. Li, Y. *et al.* Rational pore-window size control in three Cu-MOFs with different pore environments for efficient capture of the greenhouse gas SF_6. *J. Solid. State. Chem.* **329**, 124443 (2024).
22. Fu, W. *et al*. Highly-efficient separation of SF_6/N_2 and NF_3/N_2 with record selectivity on one-step synthesized carbon nanosheet. *Sep. Purif. Technol.* **330**, 125496 (2024).
23. Zheng, S. *et al*. Methyl-functionalized microporous metal-organic framework for efficient SF_6/N_2 separation. *Sep. Purif. Technol.* **318**, 123957 (2023).